Para metallation of 3-acetyl-chromen-2-one Schiff bases in tetranuclear palladacycles: Focus on their biomolecular interaction and *in vitro* cytotoxicity

G. Kalaiarasi,[a] S. Dharani,[a] V. M. Lynch[b] and R. Prabhakaran[a*]

[a]*Department of Chemistry, Bharathiar University, Coimbatore, 641 046, India.*
[b]*Department of Chemistry, University of Texas, Austin, TX 78712-1224, USA.*
*Corresponding author e-mail: rpnchemist@gmail.com (R. Prabhakaran)

SUPPORTING INFORMATION

Materials and methods

Ethidium bromide (EB), Serum albumins (BSA/HSA), Calf Thymus DNA (CT-DNA) were purchased from HiMedia and used as received. Melting points were measured in a Lab India apparatus. Infrared (IR) spectra were measured on a JASCO FT-IR 4100 instrument as KBr pellets between 400–4000 cm^{-1}. The electronic spectra of the compounds were recorded in dichloromethane using a Spectrophotometer (JASCO V-630) in the 200-800 nm range. Emission spectra were recorded by using JASCO FP 6600 Spectrofluorimeter. ^1H NMR spectra were recorded in DMSO at room temperature with a Bruker 400 MHz instrument chemical shift relative to tetramethylsilane (TMS).

X-ray Crystallography

Hydrogen bonding in complexes 1-4

In the tetrameric crystal structure of **1**, each monomeric unit showed three hydrogen bonds: The hydrogen atom of H(3A) of amino group N(3)–H(3A) is engaged in intermolecular hydrogen bonding with oxygen atom O(1B) of the DMF molecule, which came from solvent of crystallisation (O(1B)–N(3A)=3.15(4)). The hydrogen atom H(3B) of amino group N(3)–H(3B) is involved in intermolecular hydrogen bonding with ring carbonyl oxygen atom O(2) of a second molecule and the ring carbonyl oxygen atom O(2) of the first molecule involved in hydrogen bond with hydrogen atom H(3B) of the amino group of the another molecule. This intermolecular hydrogen bonding leads to an unremitting 3D chain formation (Fig. S13) at four ends of the tetramer with a distance of 2.971(8) Å [O(2)–N(3)=2.971(8); N(3)–H(3B)···O(2) = 172.00(8)°] (Table S3).

In complex **2**, the molecular packing suggests that the stabilization of the lattice may be due to eight intermolecular hydrogen bonds, each monomeric unit involving the two hydrogen bonds: one hydrogen bond between the ring carbonyl oxygen atom O(2) of the first molecule and hydrogen (H3) atom of the terminal N(3)–H(3) group of the second molecule and second hydrogen bond involves the hydrogen (H3) atom of the terminal N(3)–H(3) group of the first molecule and ring carbonyl oxygen atom O(2) of the another molecule (N(3)–O(2), O(2)–N(3) is 2.895 Å). All the eight intermolecular hydrogen bondings led to give a 3D layer structure to the complex **2** (Fig. S14).

The presence of four intermolecular hydrogen bondings in complex **3** creates a 2D network (Fig. S15; Table S3). In tetrameric unit of complex **3**, one of the monomeric unit involved in intermolecular hydrogen bonding with carbonyl oxygen atom O(2) and the hydrogen atom H(12) of terminal N(12)–H(12) group of second molecule and the hydrogen atom H(12) of terminal N(12)–H(12) group in same monomeric unit engaged in intermolecular hydrogen bonding with carbonyl atom O(2) of the another molecule. The hydrogen atom H(12) of terminal N(12)–H(12) group in second monomeric unit is involved in intermolecular hydrogen bonding with carbonyl oxygen atom O(2) of a second molecule. Third monomeric unit involving the hydrogen bond between the ring carbonyl oxygen atom O(2) and hydrogen (H3) atom of the terminal N(3)–H(3) group of the second molecule. In complex **4,** an intermolecular hydrogen bonding was found between the terminal nitrogen and the oxygen atom of the DMF [N(3)...O(3) (2.858 Å); N(3)–H(3)···O(3)=174.56 °] which came through the solvent of crystallization (Fig. S16; Table S3).

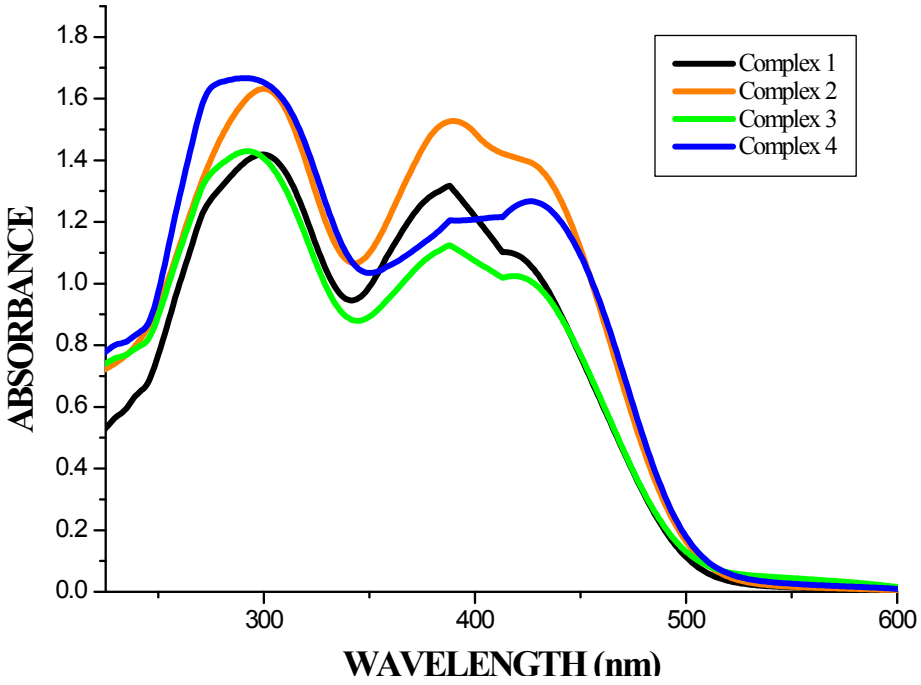

Fig. S1 UV-Vis spectra of the complexes **1-4**

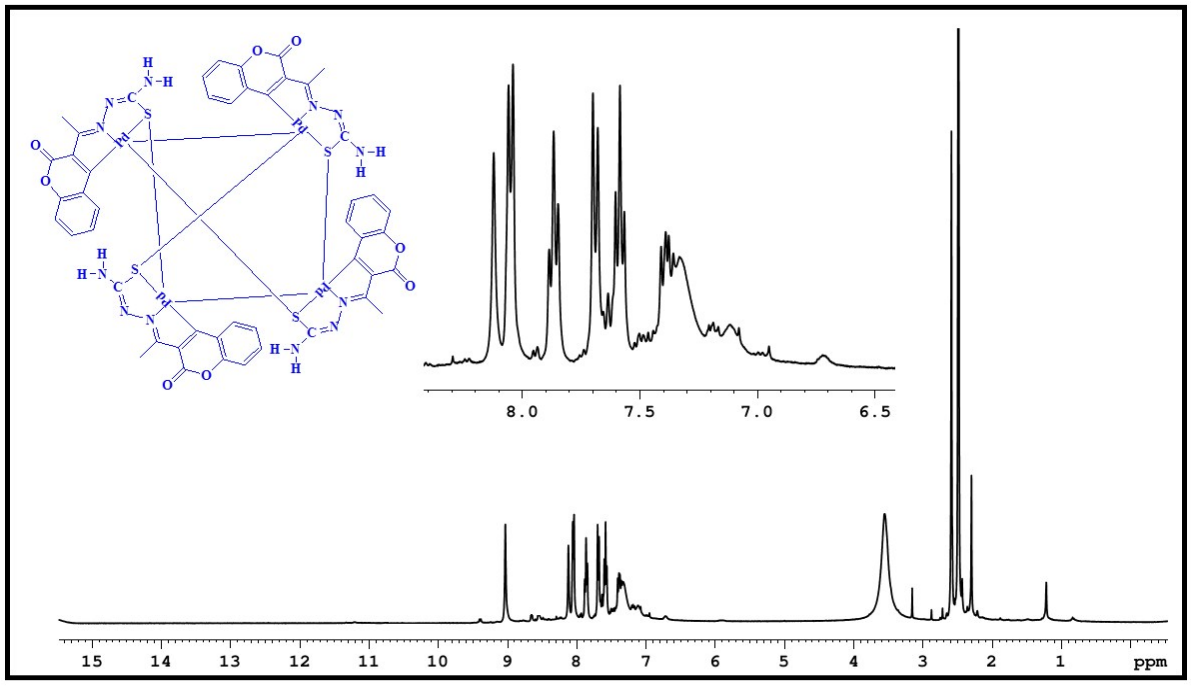

Fig. S2 ^{1}H-NMR spectrum of **[{Pd(3MAC-tsc)}$_4$] (1)**

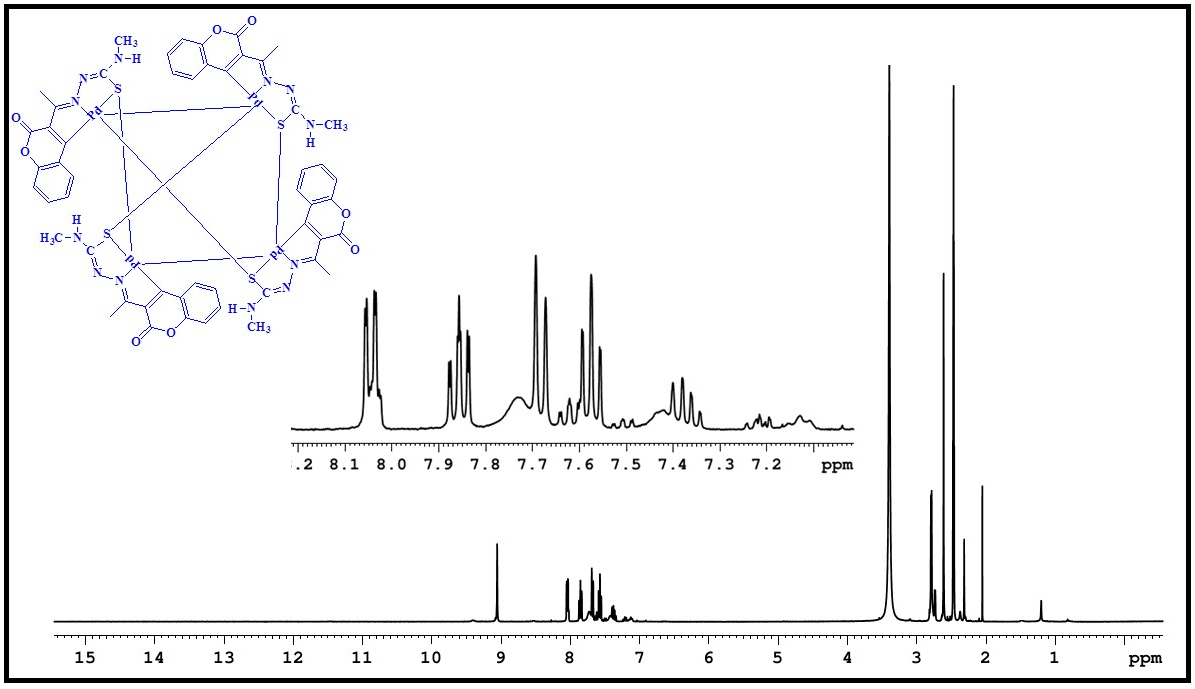

Fig. S3 ^{1}H-NMR spectrum of **[{Pd(3MAC-mtsc)}$_4$] (2)**

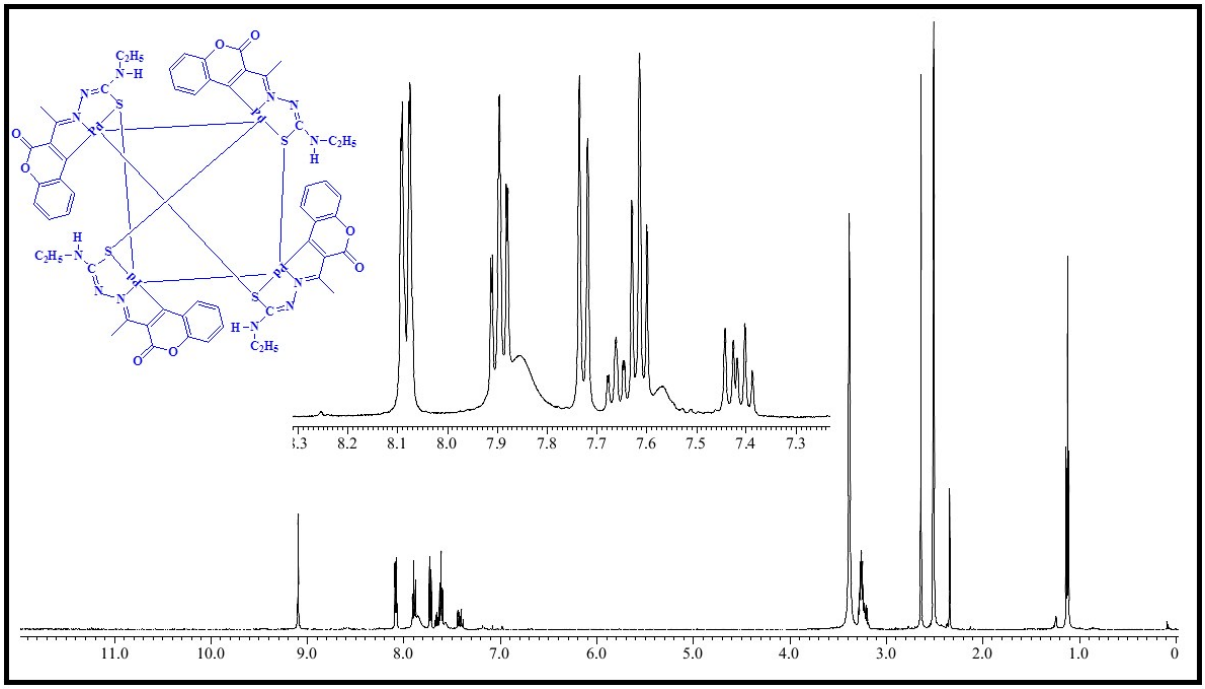

Fig. S4 ^{1}H-NMR spectrum of **[{Pd(3MAC-etsc)}$_4$] (3)**

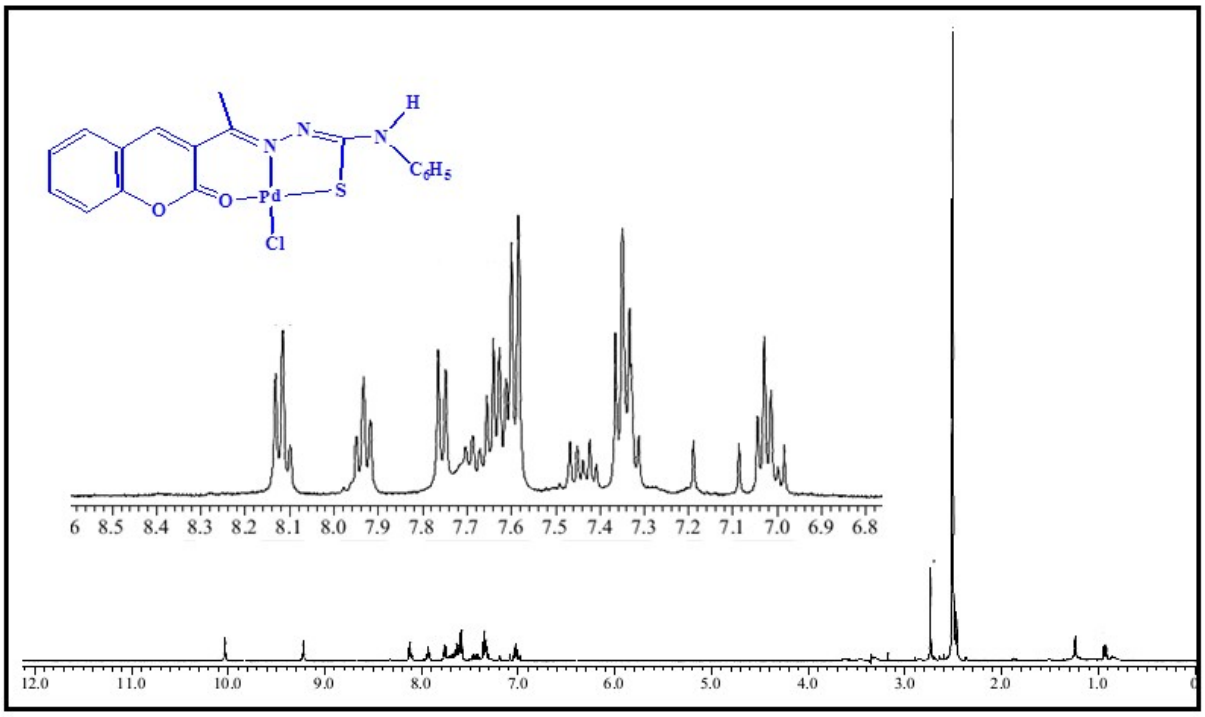

Fig. S5 ^{1}H-NMR spectrum of **[Pd(H-3MAC-ptsc)Cl] (4)**

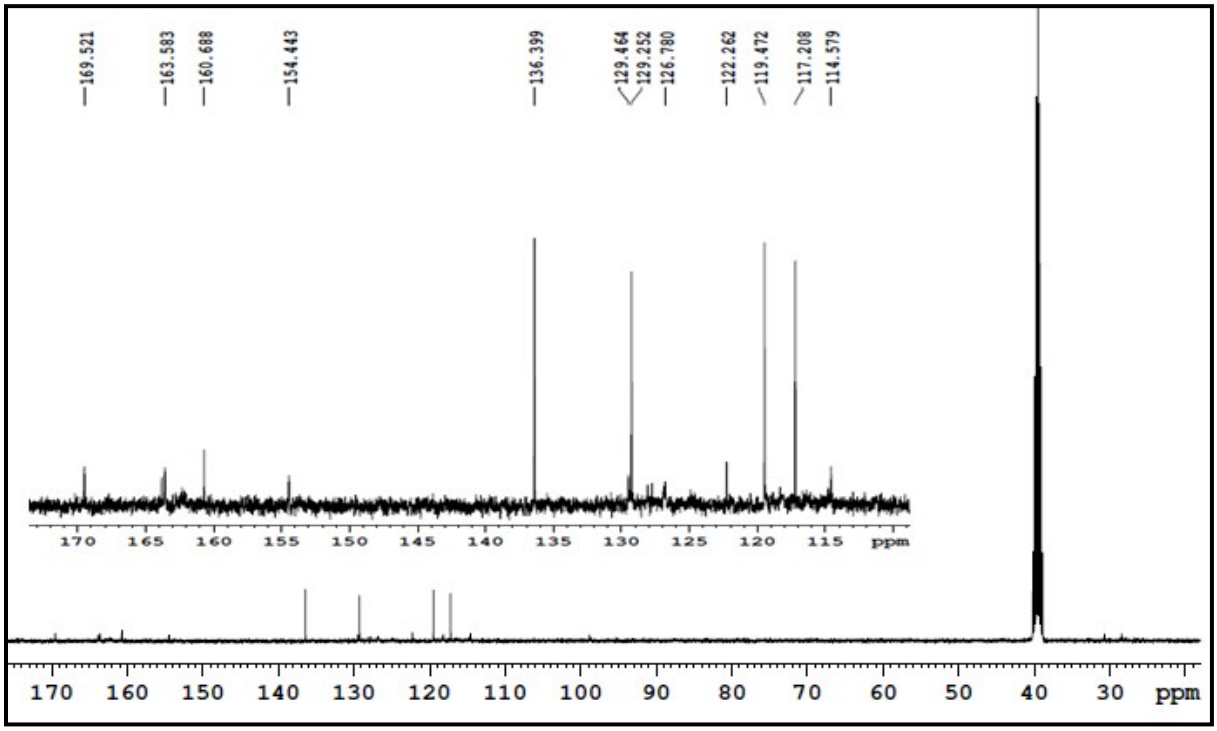

Fig. S6 ^{13}C-NMR spectrum of **[{Pd(3MAC-tsc)}$_4$] (1)**

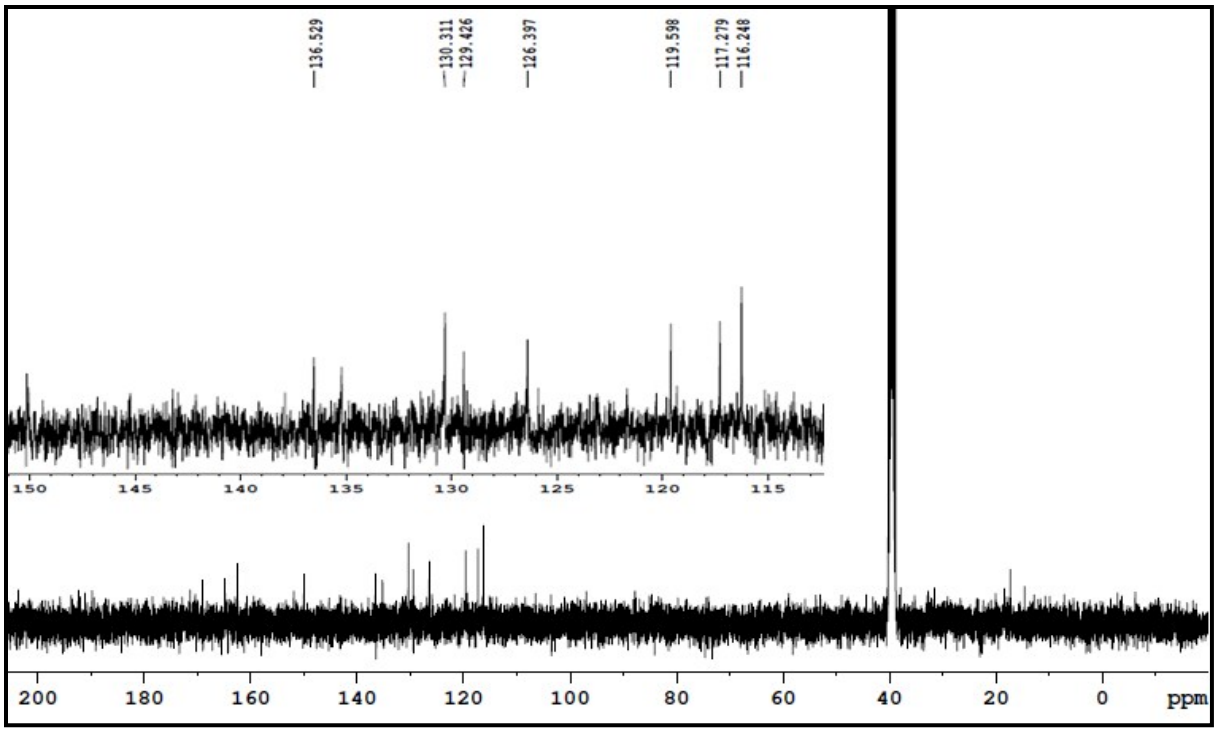

Fig. S7 ^{13}C-NMR spectrum of **[{Pd(3MAC-mtsc)}$_4$] (2)**

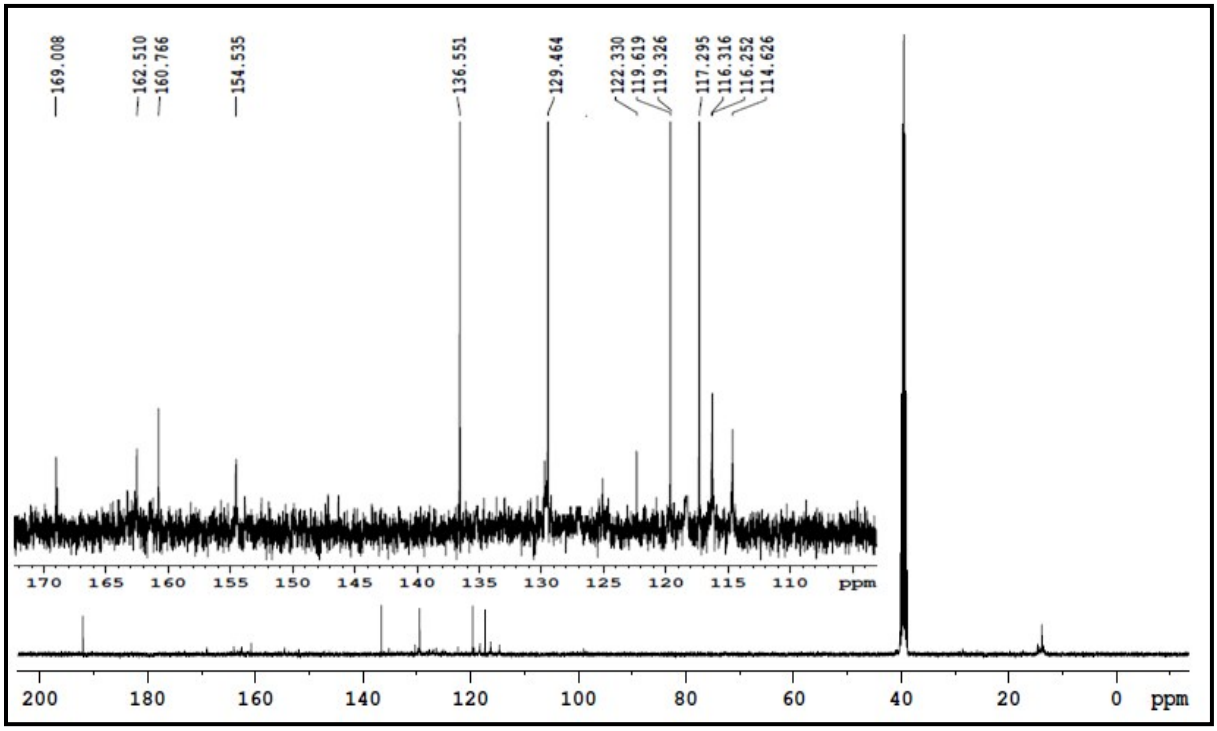

Fig. S8 ^{13}C-NMR spectrum of **[{Pd(3MAC-etsc)}$_4$] (3)**

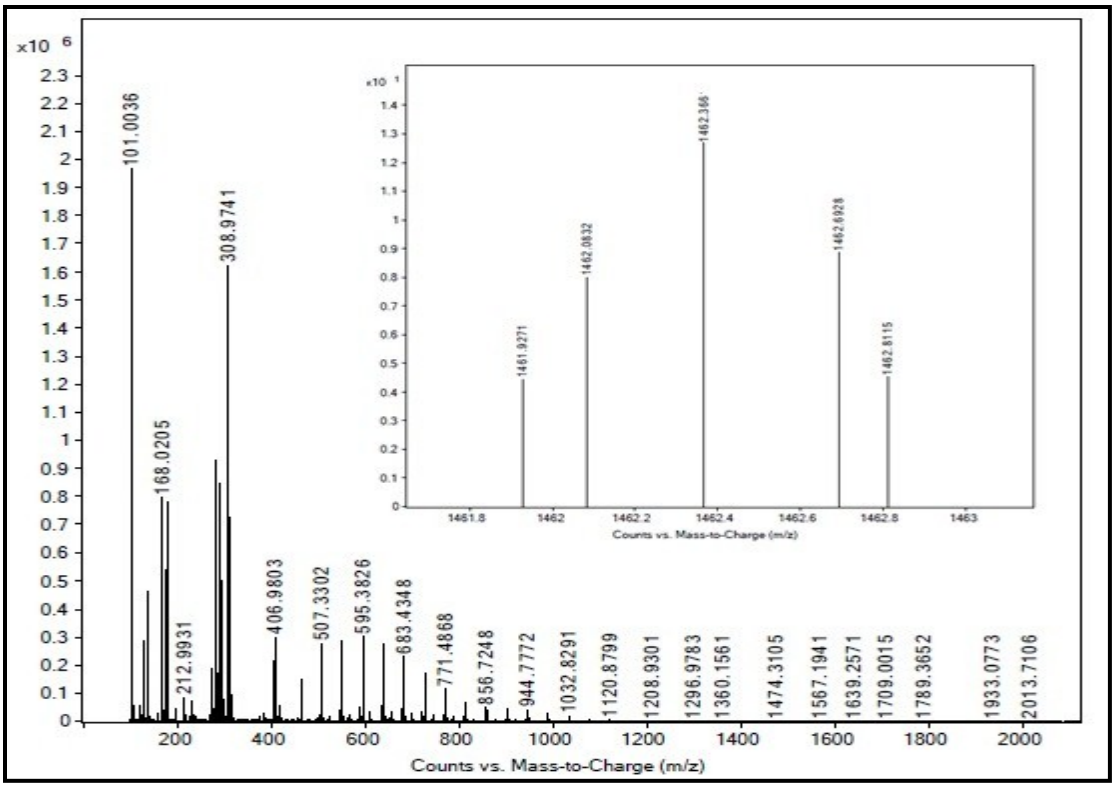

Fig. S9 ESI-MS of complex **1 [{Pd(3MAC-tsc)}$_4$]**

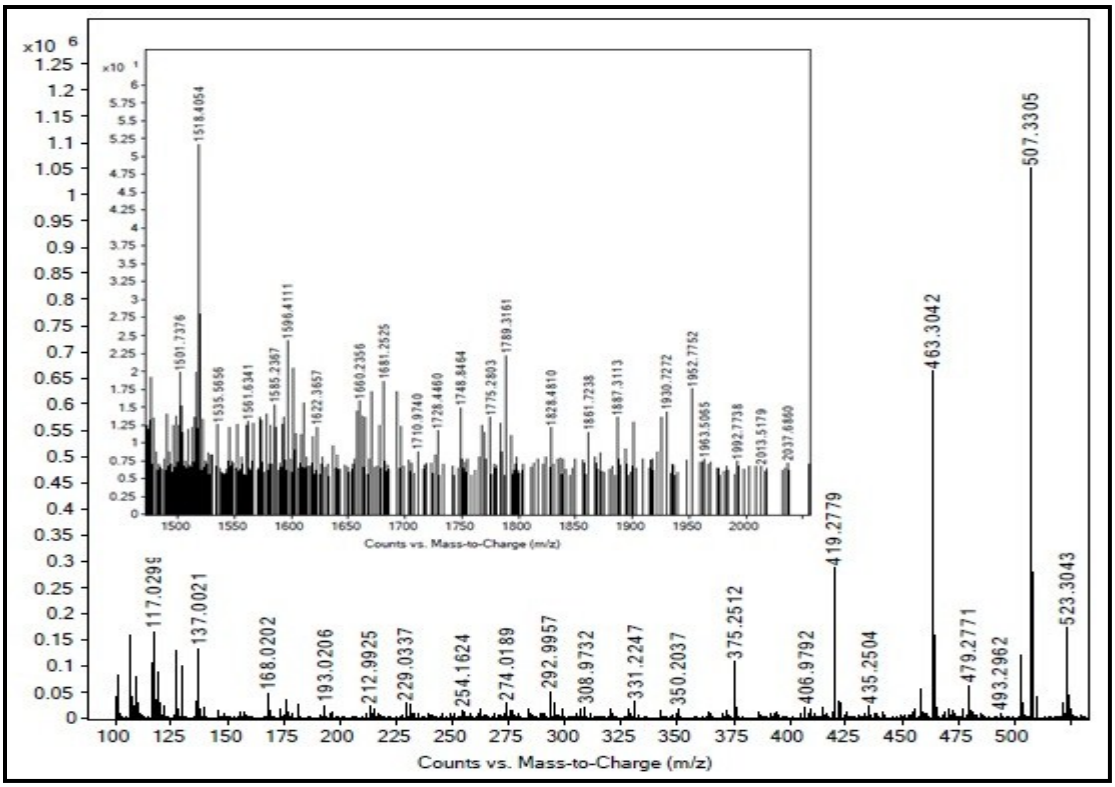

Fig. S10 ESI-MS of complex **2 [{Pd(3MAC-mtsc)}$_4$]**

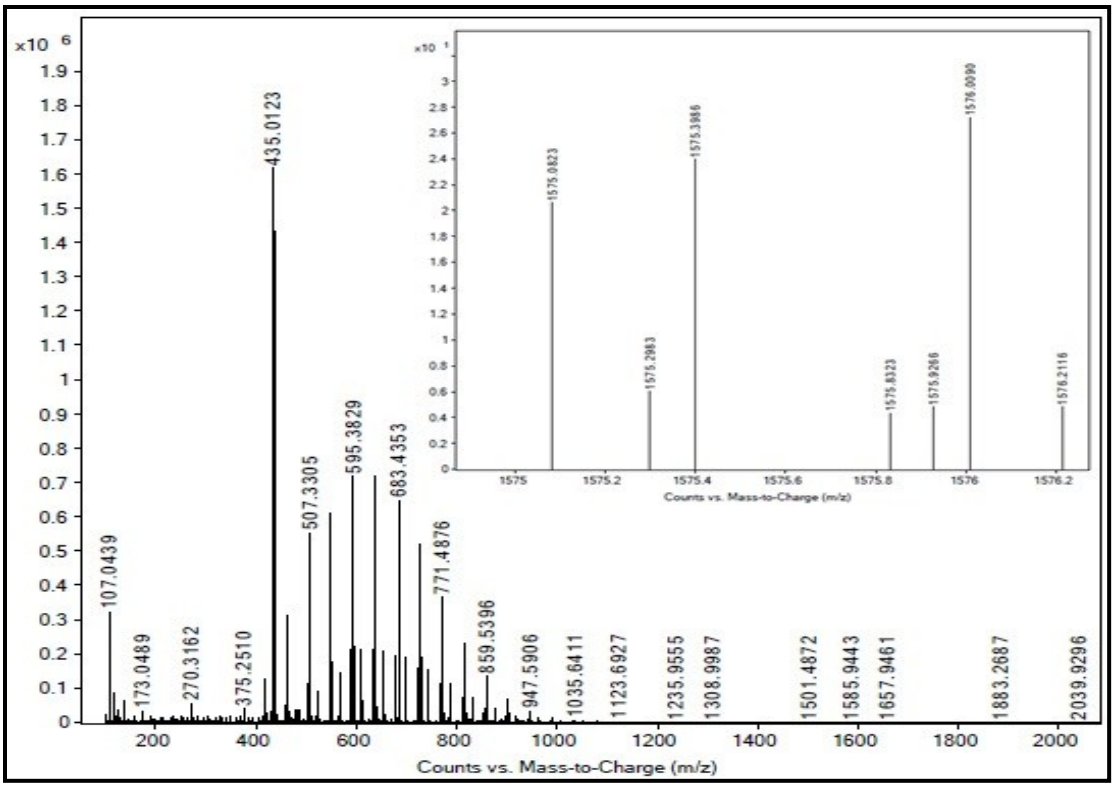

Fig. S11 ESI-MS of complex **3**‖**[{Pd(3MAC-etsc)}$_4$]**

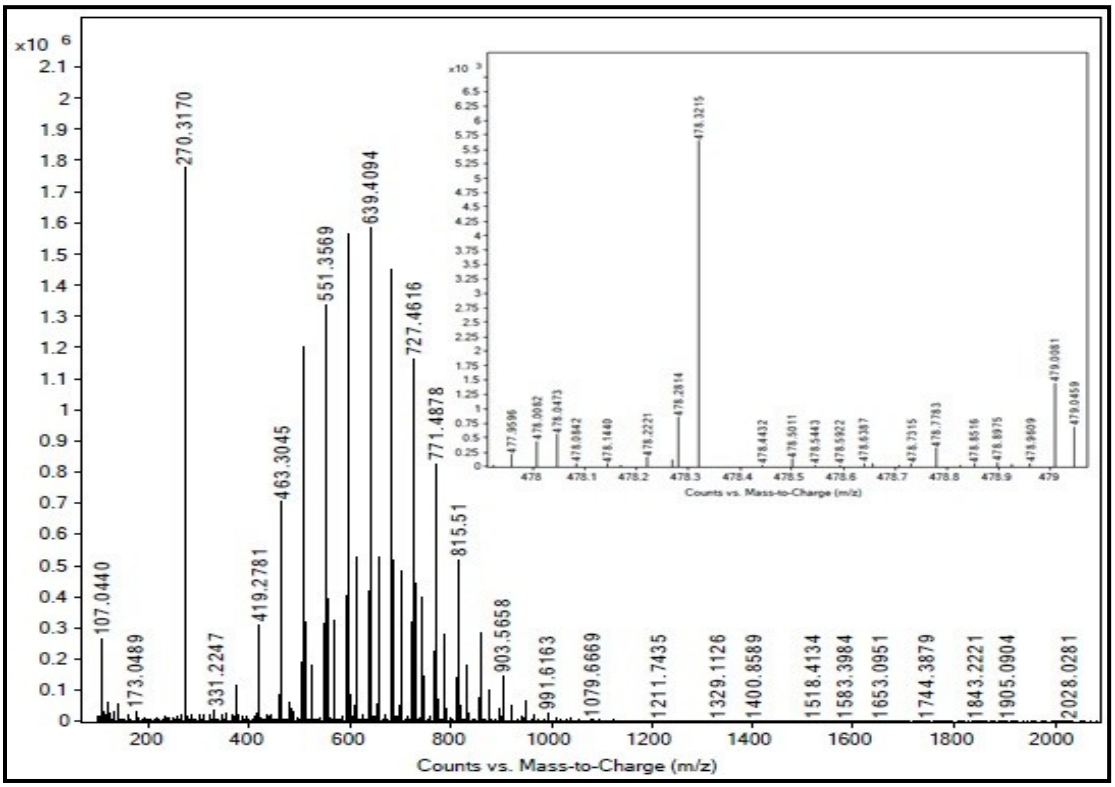

Fig. S12 ESI-MS of complex **4 [Pd(H-3MAC-ptsc)Cl]**

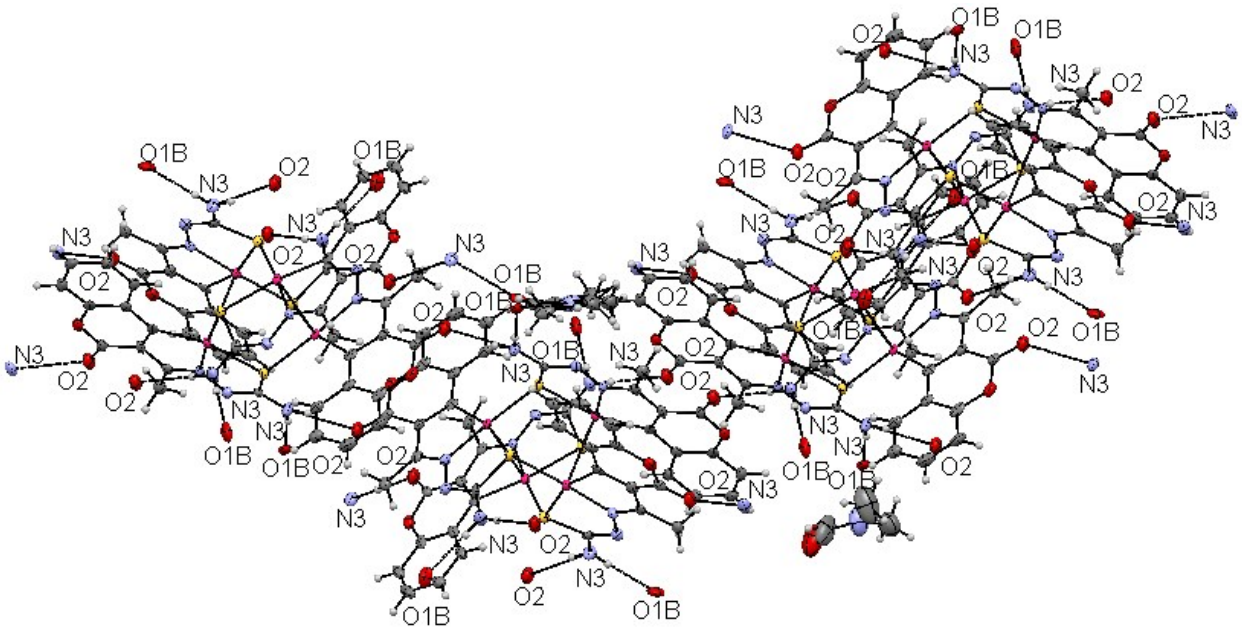

Fig. S13 ORTEP diagram of the complex **[{Pd(3MAC-tsc)}$_4$] (1)** with hydrogen bonding

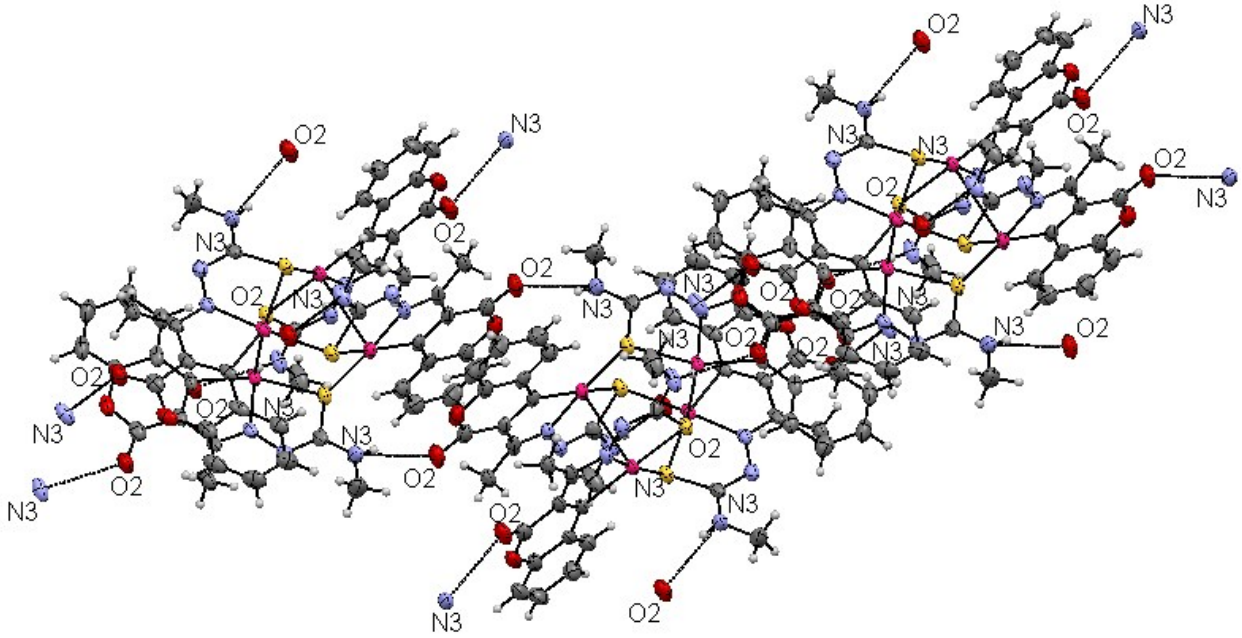

Fig. S14 ORTEP diagram of the complex **[{Pd(3MAC-mtsc)}$_4$] (2)** with hydrogen bonding

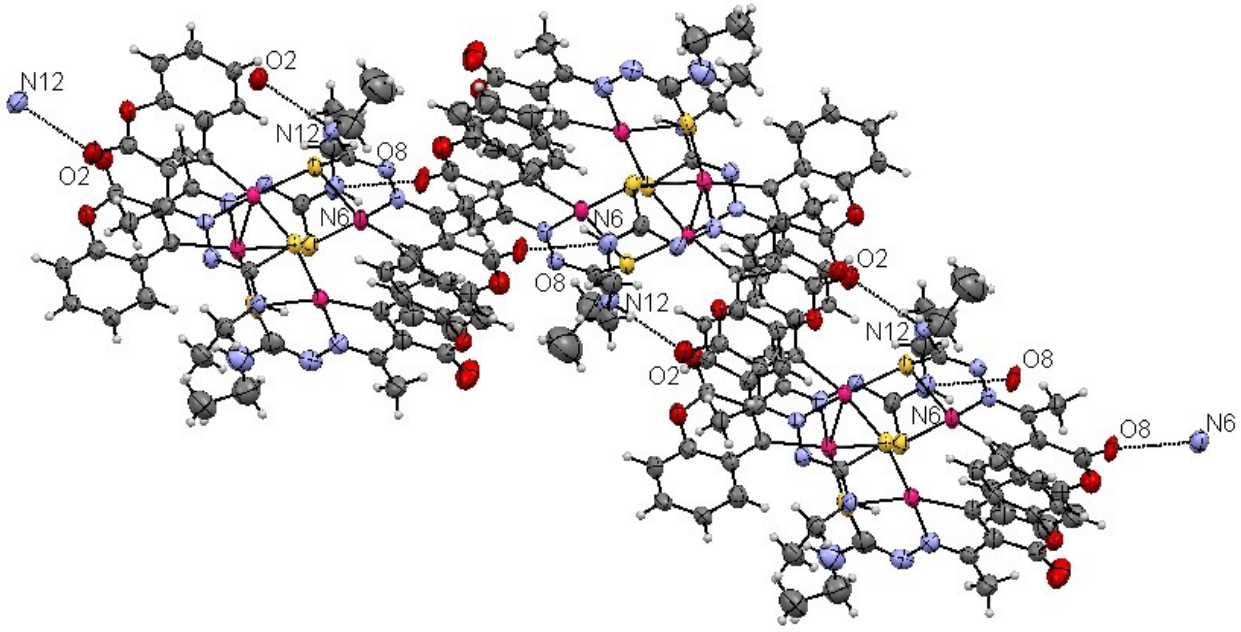

Fig. S15 ORTEP diagram of the complex **[{Pd(3MAC-etsc)}$_4$] (3)** with hydrogen bonding

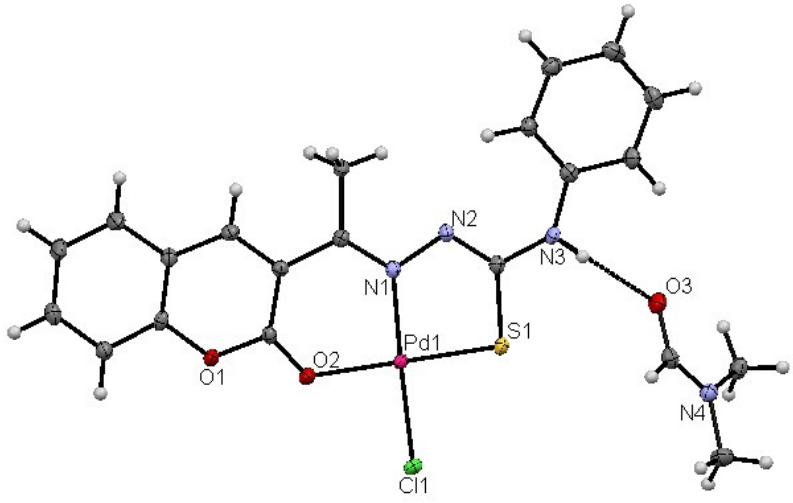

Fig. S16 ORTEP diagram of the complex **[Pd(H-3MAC-ptsc)Cl] (4)** with hydrogen bonding

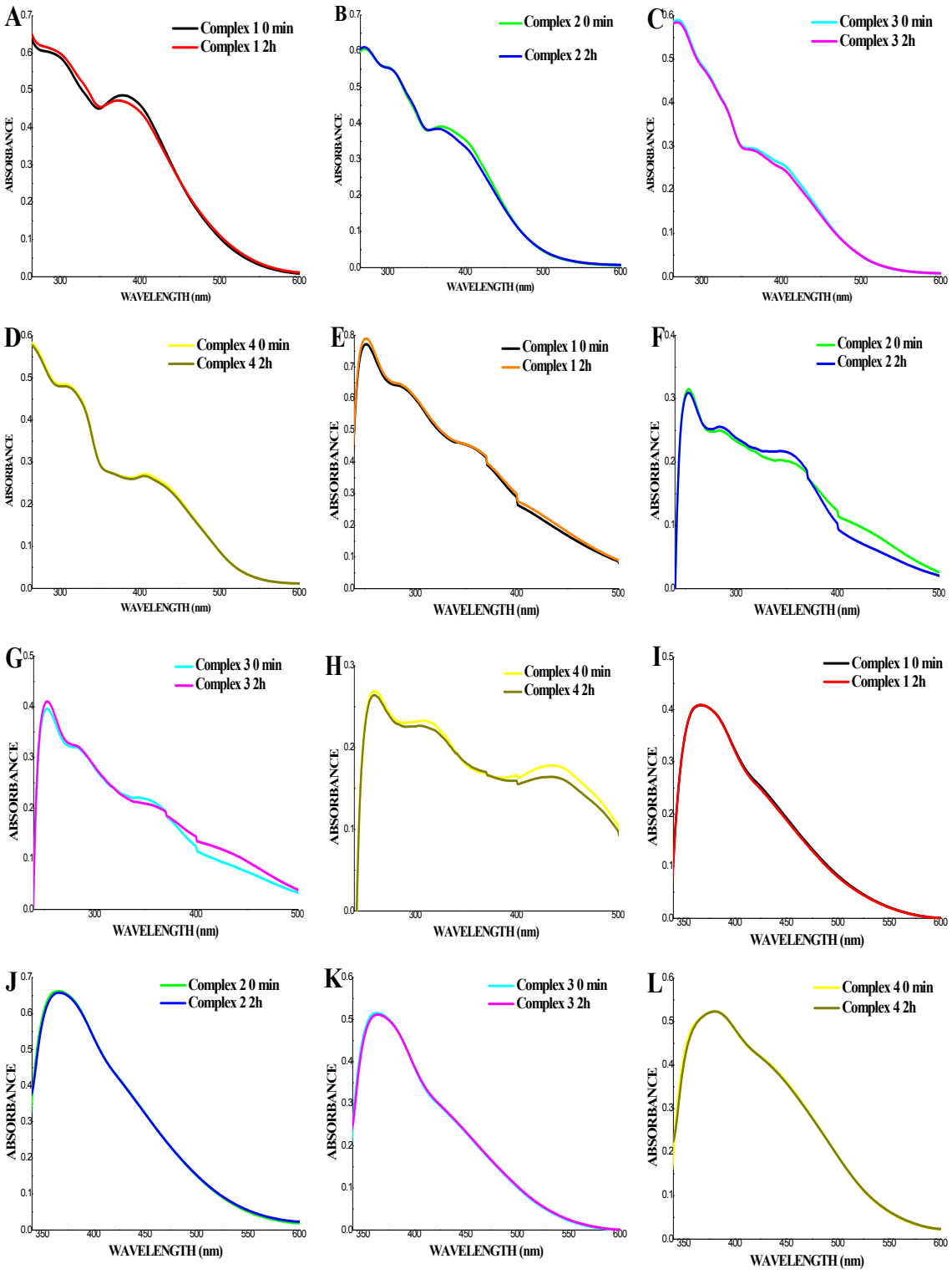

Fig. S17 Stability studies of the complexes using UV-Vis absorption spectroscopic technique. A, B, C and D - absorption spectra of the complexes **1-4** in 99:1 H_2O:DMSO; E, F, G and H - absorption spectra of the complexes **1-4** in 99:1 tris HCl:DMSO; I, J, K and L - absorption spectra of the complexes **1-4** in 99:1 phosphate buffer:DMSO

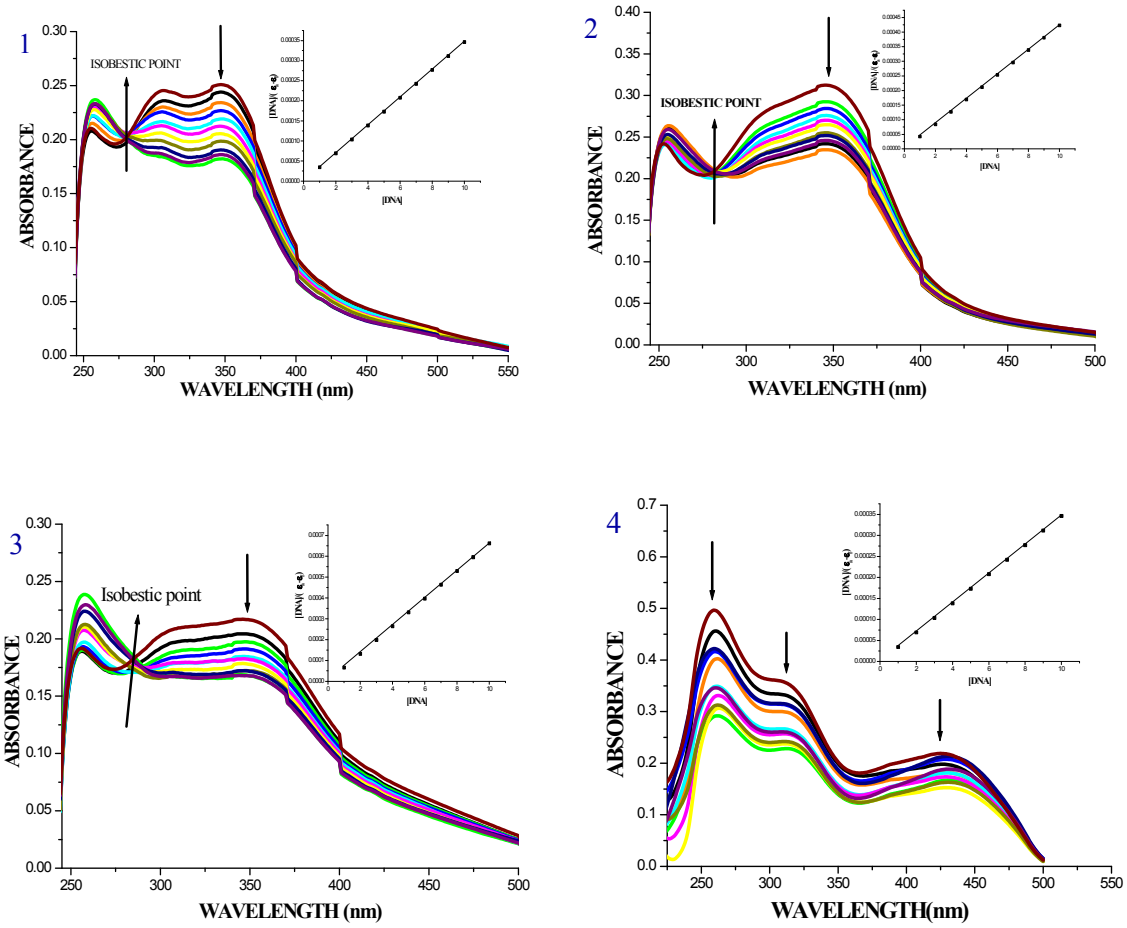

Fig. S18 Absorption titration spectra of complexes (**1-4**) (10 μM) with increasing concentrations (1-10 μM) of CT-DNA (tris HCl buffer, pH 7.2). Inset: Binding isotherms of the complexes (**1-4)** with CT-DNA

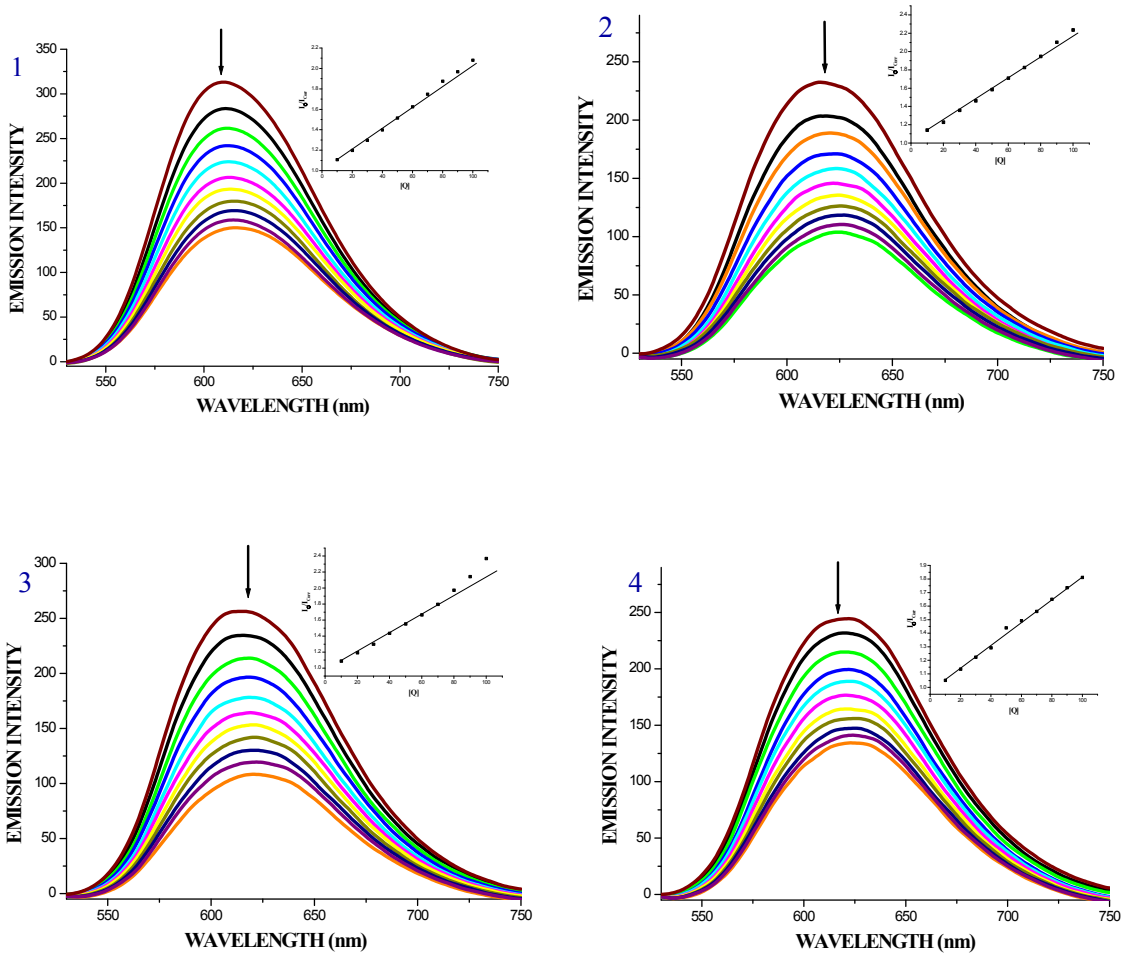

Fig. S19 The emission spectra of the DNA–EB system (λ_{exc} = 515 nm, λ_{emi} = 530–750 nm), in the presence of complexes **1-4**. [DNA] = 10 μM, [complex] = 10–100 μM, [EB] = 10 μM. The arrow shows the emission intensity changes upon increasing complex concentration. Inset: Stern−Volmer plot of the fluorescence titration of the complexes (**1-4**) (10-100 μM) with DNA-EB (10 μM).

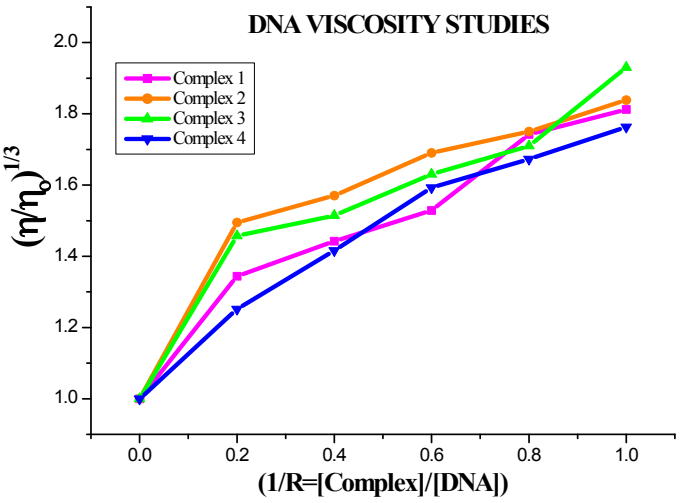

Fig. S20 Effect of the complexes (**1-4**) on the viscosity of CT-DNA

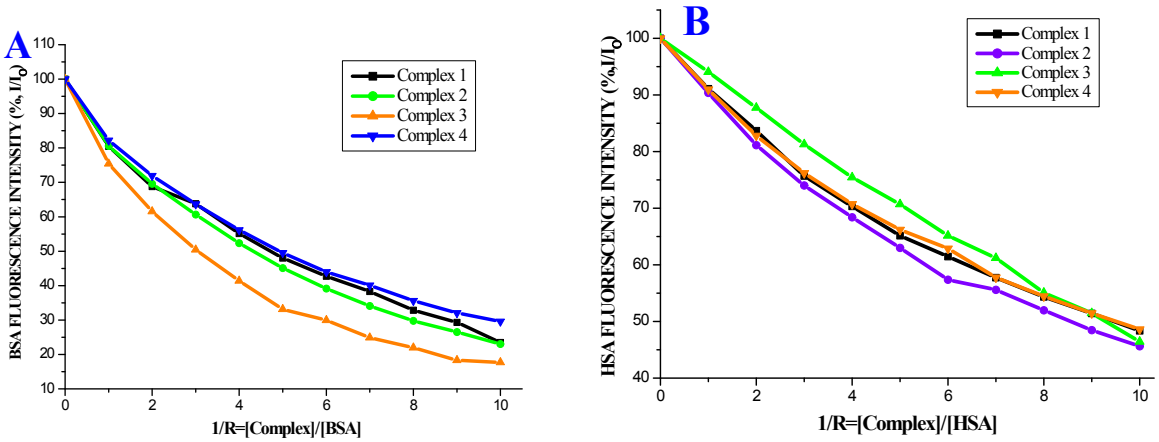

Fig. S21 A) Plot of % relative fluorescence intensity (% I/I_o) vs r (1/R=[Complex]/[BSA]) **B)** Plot of % relative fluorescence intensity (% I/I_o) vs r (1/R=[Complex]/[HSA])

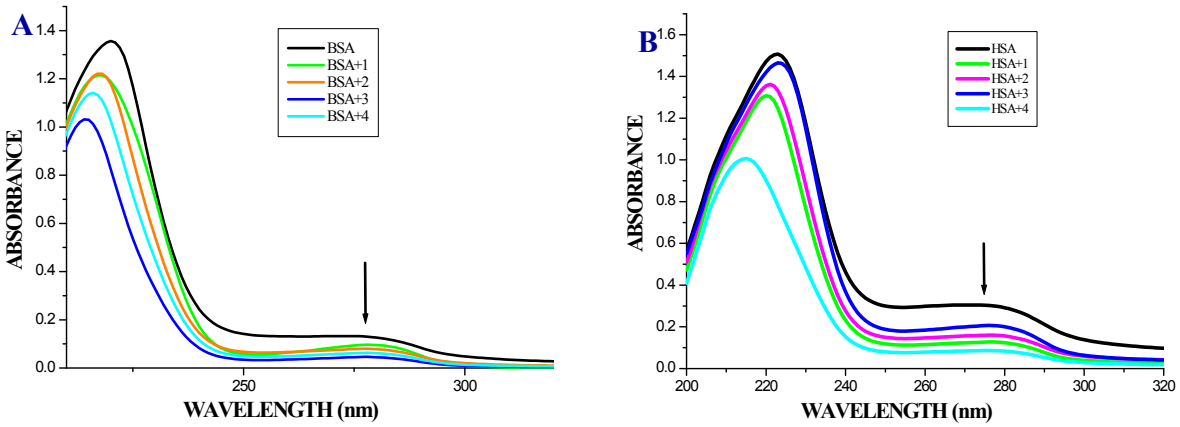

Fig. S22 A) Absorption spectra in the absence and presence of complexes (**1-4**) with BSA (1×10^{-5} M); **B)** Absorption spectra in the absence and presence of complexes (**1-4**) with HSA (1×10^{-5} M)

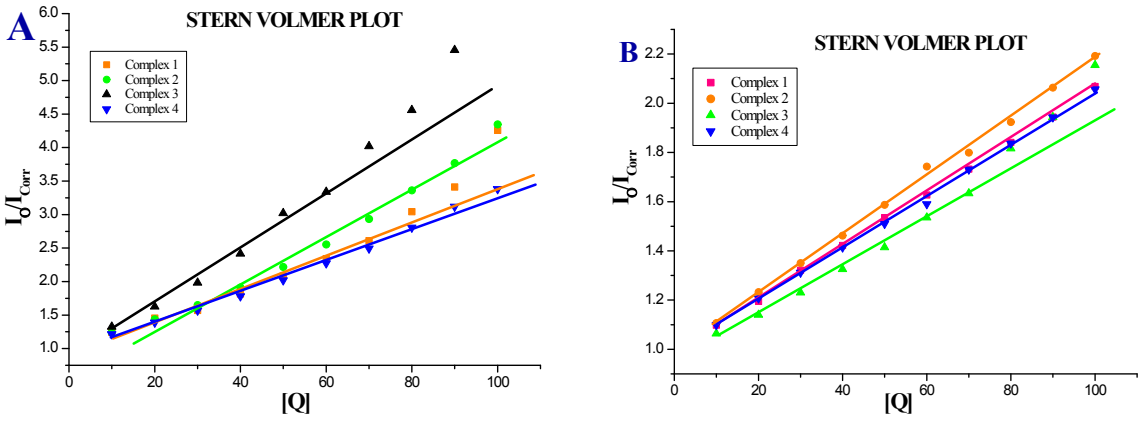

Fig. S23 A) Stern-Volmer plot of the fluorescence titration of the complexes (**1-4**) (10-100 µM) with BSA; **B)** Stern-Volmer plot of the fluorescence titration of the complexes (**1-4**) (10-100 µM) with HSA

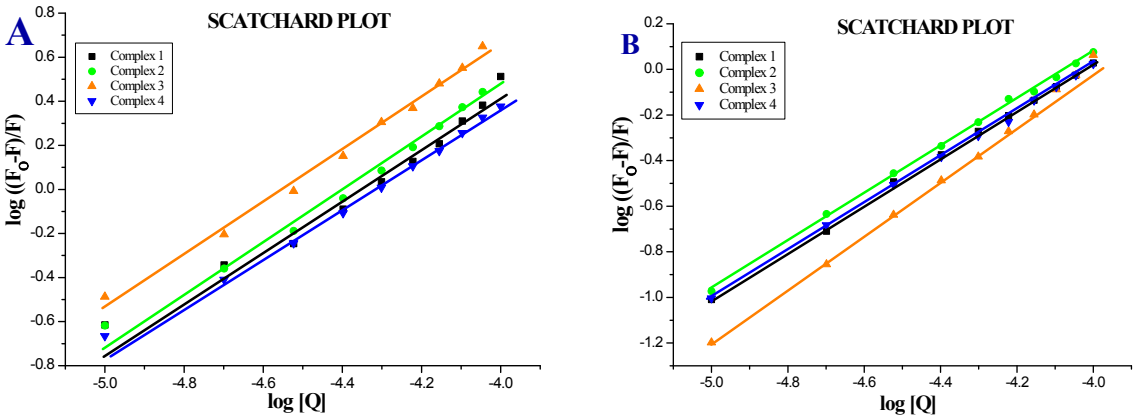

Fig. S24 A) Scatchard plot of the fluorescence titration of the complexes (**1-4**) (10-100 µM) with BSA (10 µM); **B**) Scatchard plot of the fluorescence titration of the complexes (**1-4**) (10-100 µM) with HSA (10 µM)

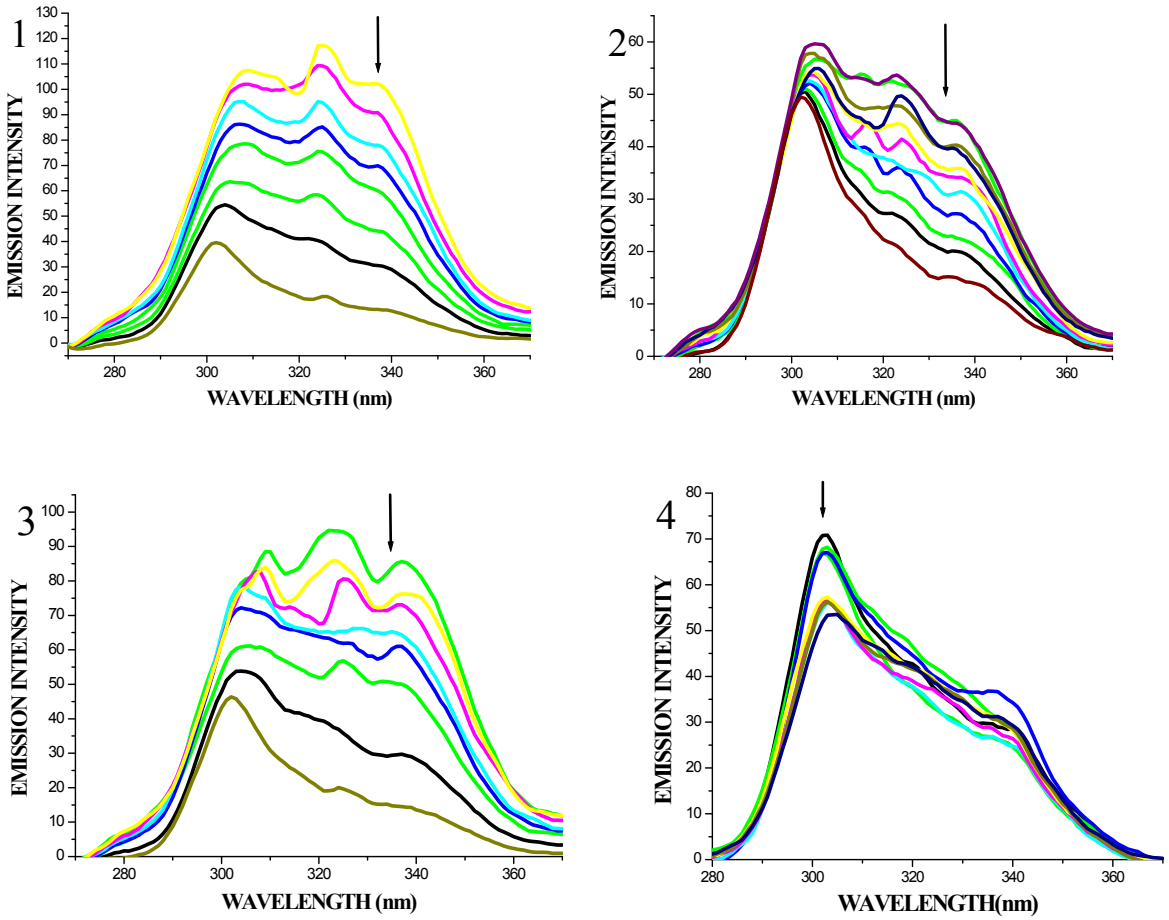

Fig. S25 Synchronous spectra of BSA (10 μM) in the presence of increasing amounts of complexes **1-4** (10–100 μM) for a wavelength difference of Δλ= 15 nm. The arrow shows the emission intensity changes upon increasing concentration of complexes.

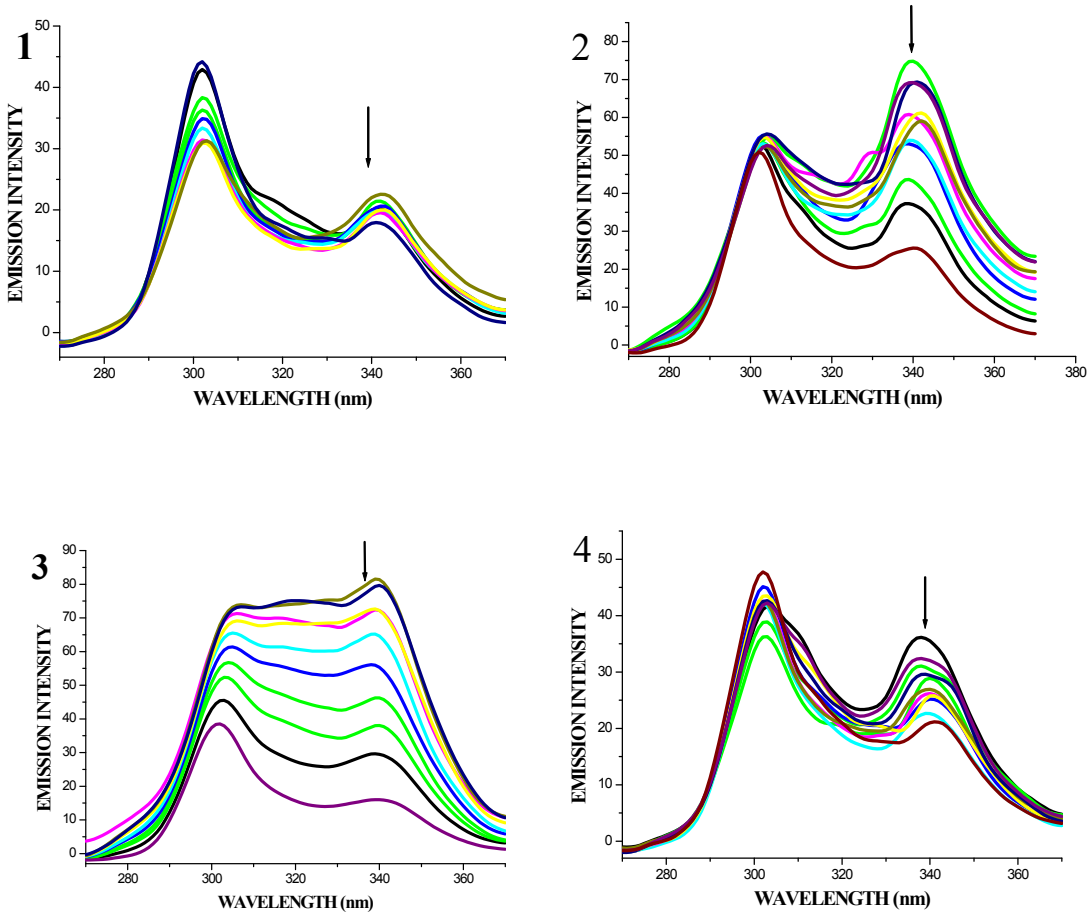

Fig. S26 Synchronous spectra of HSA (10 μM) in the presence of increasing amounts of complexes **1-4** (10–100 μM) for a wavelength difference of Δλ= 15 nm. The arrow shows the emission intensity changes upon increasing concentration of complexes.

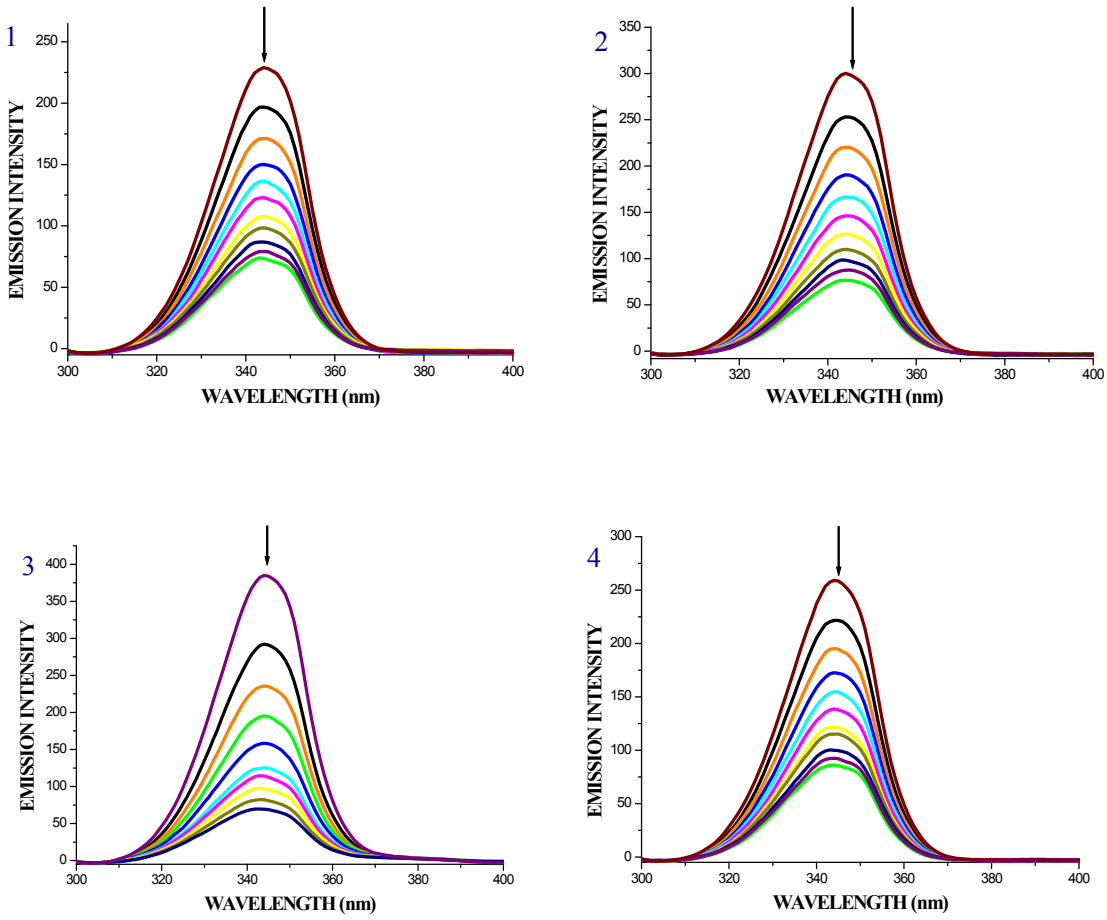

Fig. S27 Synchronous spectra of BSA (10 μM) in the presence of increasing amounts of complexes **1-4** (10–100 μM) for a wavelength difference of Δλ= 60 nm. The arrow shows the emission intensity changes upon increasing concentration of compounds.

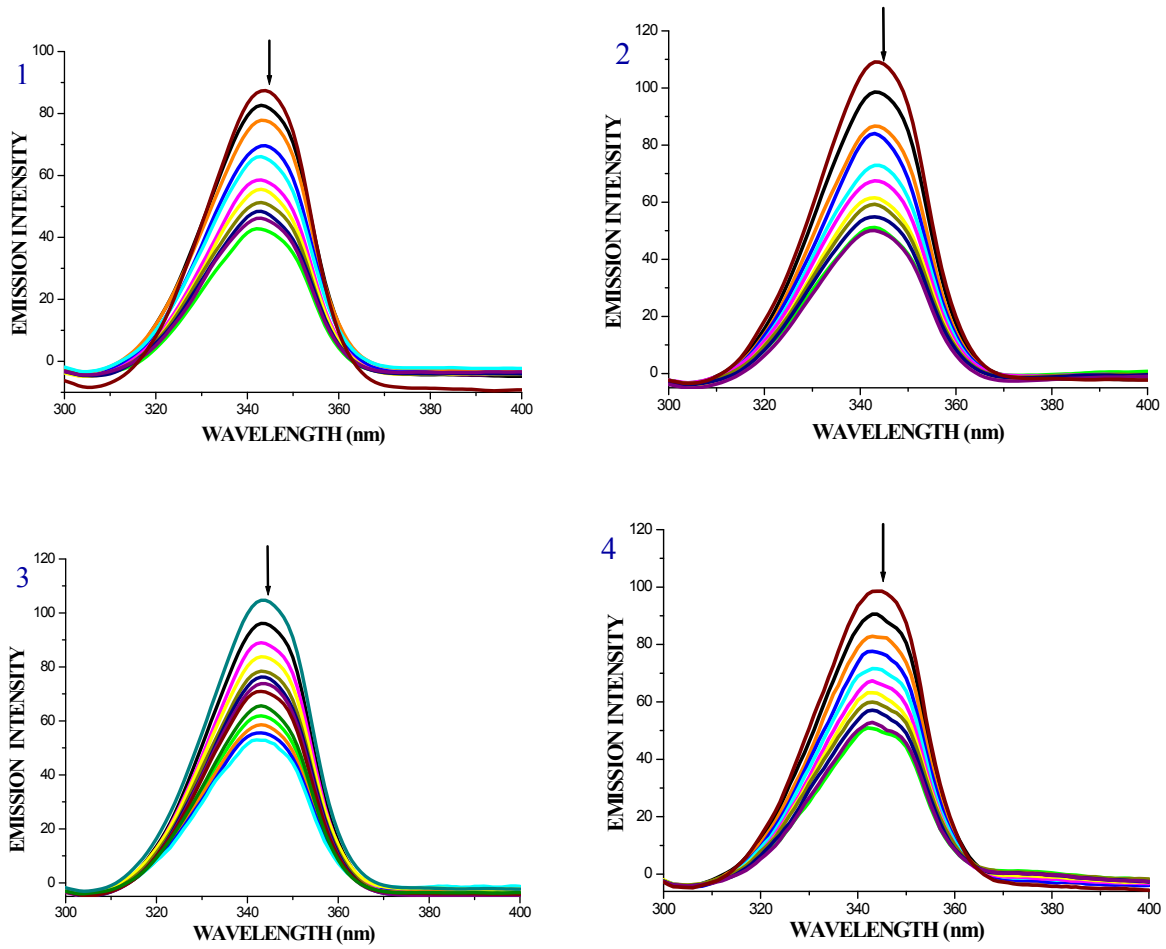

Fig. S28 Synchronous spectra of HSA (10 μM) in the presence of increasing amounts of complexes **1-4** (10–100 μM) for a wavelength difference of Δλ= 60 nm. The arrow shows the emission intensity changes upon increasing concentration of compounds.

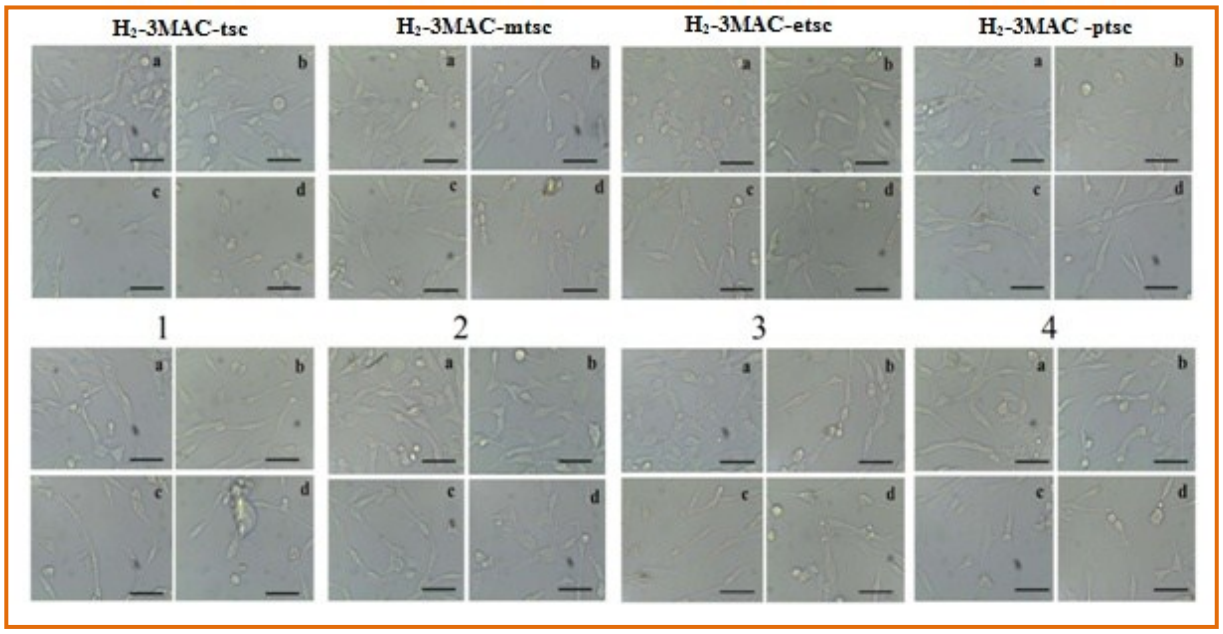

Fig. S29 Inverted light microscopic imaging: Effect of various concentrations (a - Control; b - 5 µM; c - 10 µM; d - 20 µM) of the ligands **[H_2-3MAC-Rtsc]** and complexes **1-4** on the viability of HT-29 cells

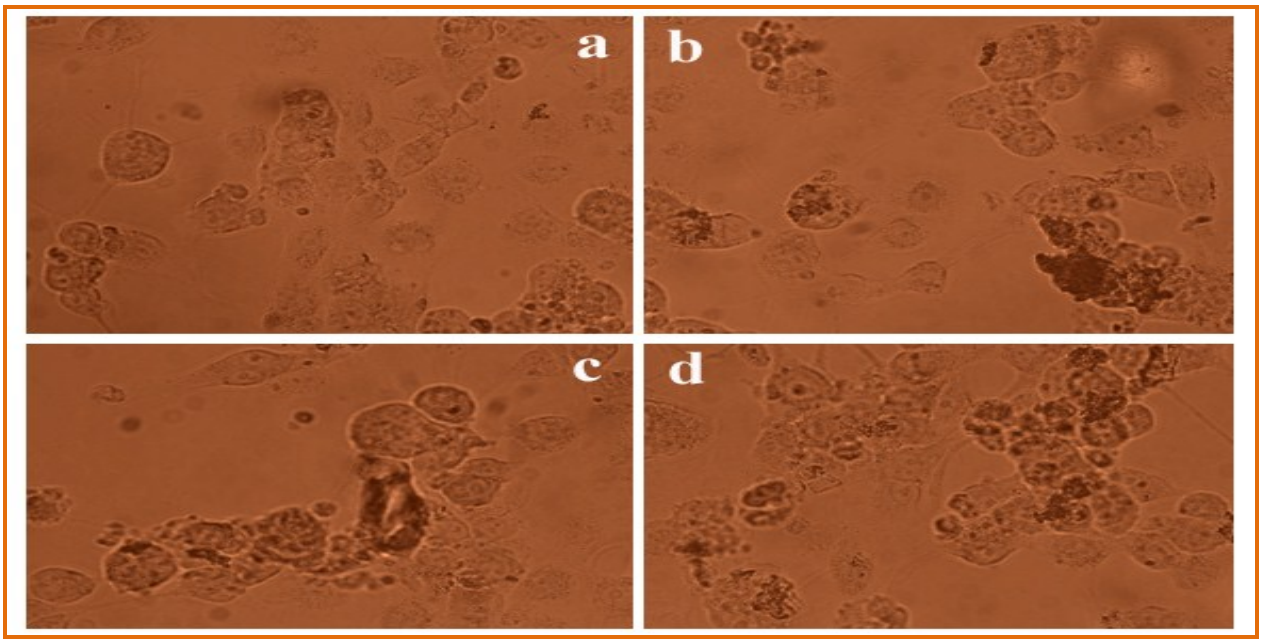

Fig. S30 Inverted light microscopic imaging: Effect of various concentrations (a - Control; b - 5 µM; c - 10 µM; d - 20 µM) of the positive control *cisplatin* on the viability of HepG2 cells.

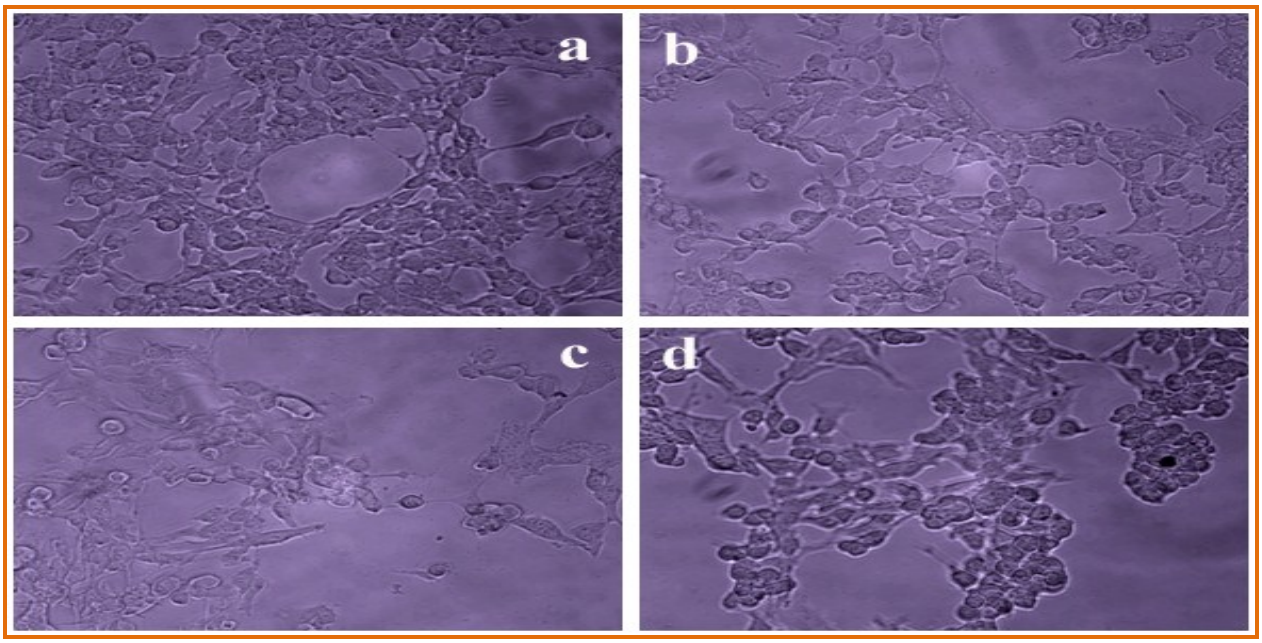

Fig. S31 Inverted light microscopic imaging: Effect of various concentrations (a - Control; b - 5 µM; c - 10 µM; d - 20 µM) of the positive control *cisplatin* on the viability of HT-29 cells.

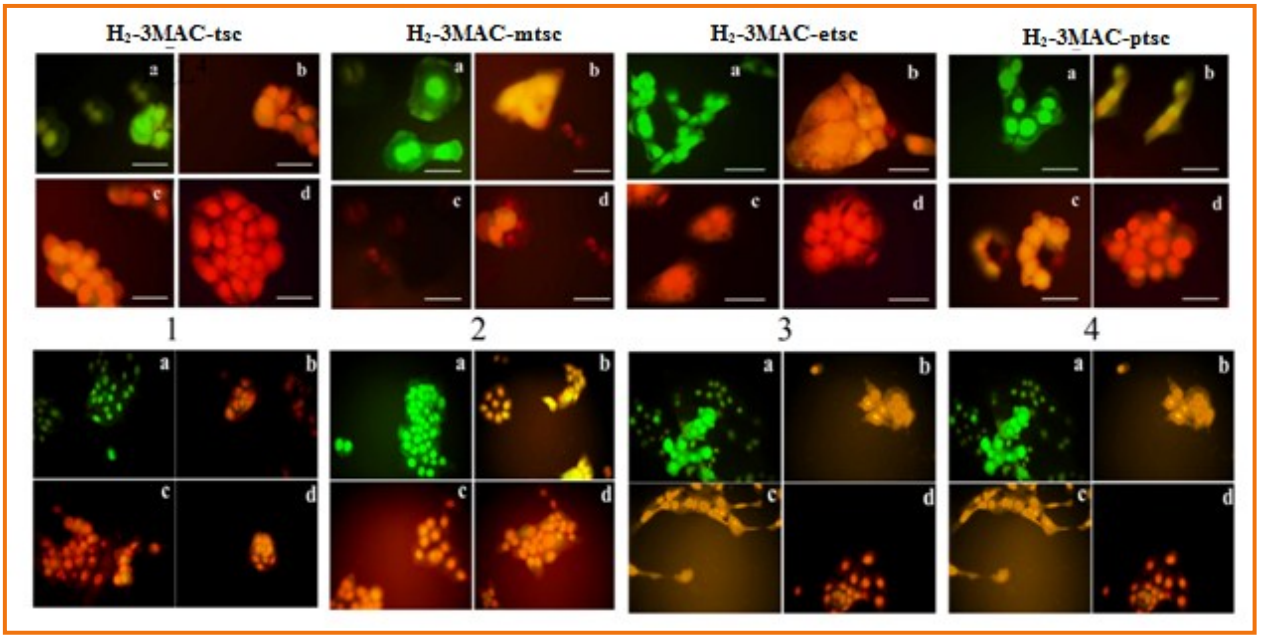

Fig. S32 AO-EB staining of HT-29 cells treated with various concentrations of the ligands **[H_2-3MAC-Rtsc]** and complexes **1-4**. (a) Control; (b), (c), (d) After 24 h treatment with 5 µM, 10 µM and 20 µM of the compounds respectively

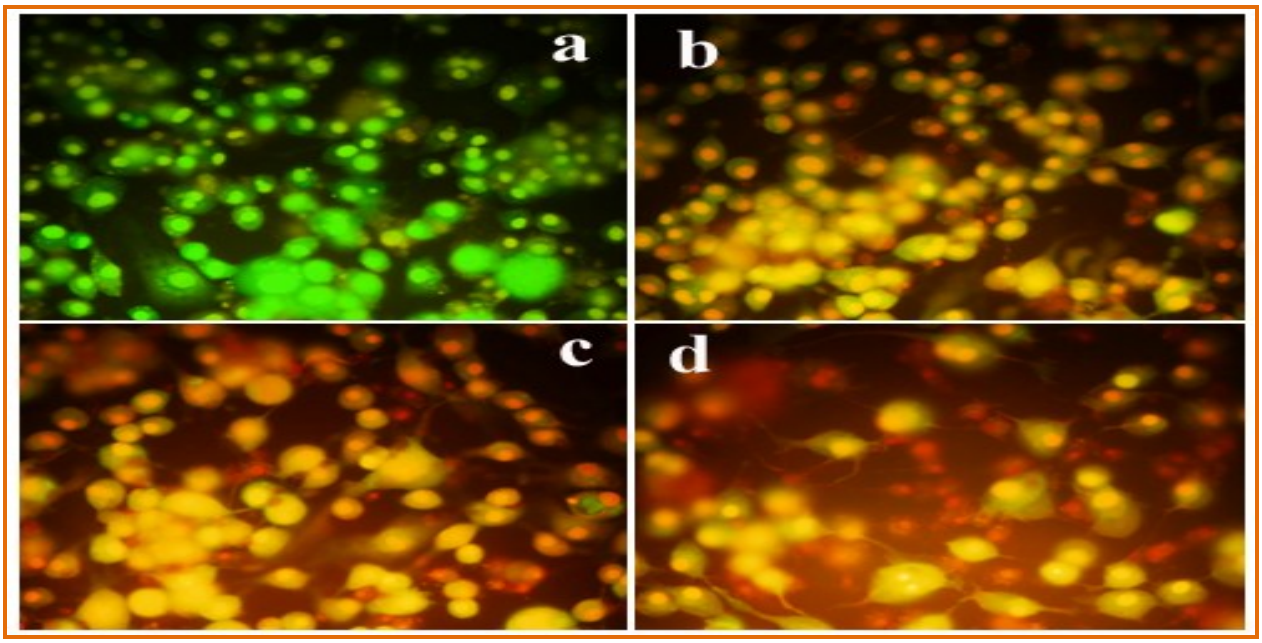

Fig. S33 AO-EB staining of HepG2 cells treated with various concentrations of the positive control *cisplatin*. (a) Control; (b), (c), (d) After 24 h treatment with 5 µM, 10 µM and 20 µM respectively.

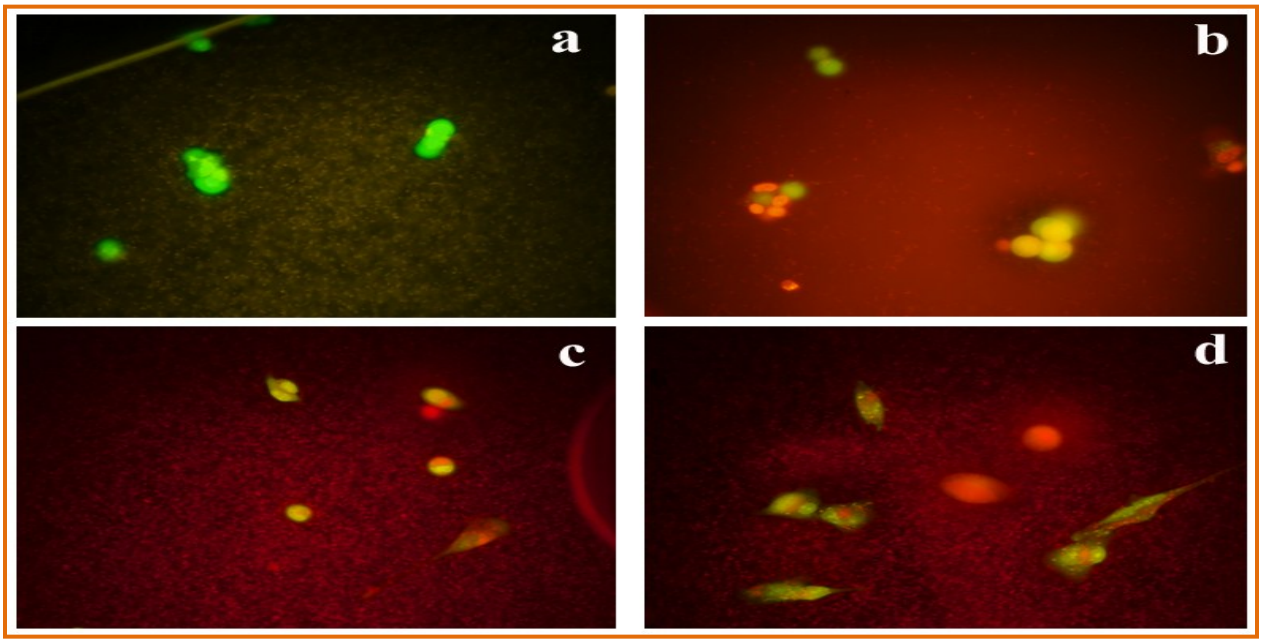

Fig. S34 AO-EB staining of HT-29 cells treated with various concentrations of the positive control *cisplatin*. (a) Control; (b), (c), (d) After 24 h treatment with 5 µM, 10 µM and 20 µM respectively.

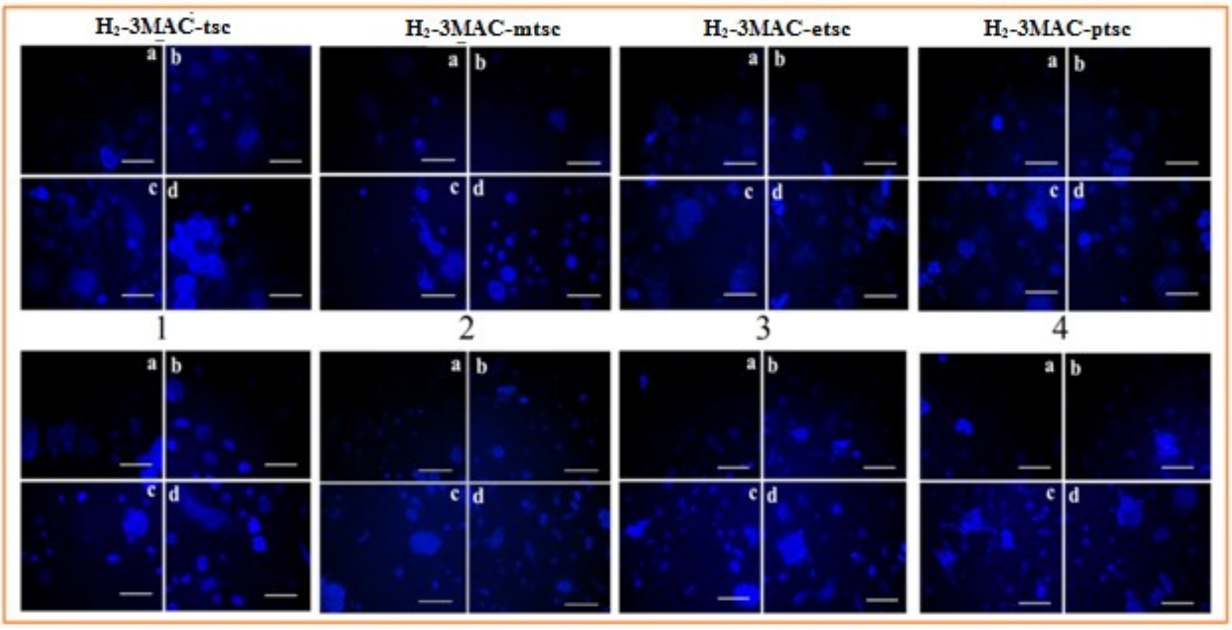

Fig. S35 Nuclear morphology of HT-29 cells stained with DAPI. HT-29 cells were treated with ligands **[H_2-3MAC-Rtsc]** and complexes **1-4** for 24 h and stained with DAPI. (a) Control; (b), (c), (d) After 24 h treatment with 5 µM, 10 µM and 20 µM of the compounds respectively

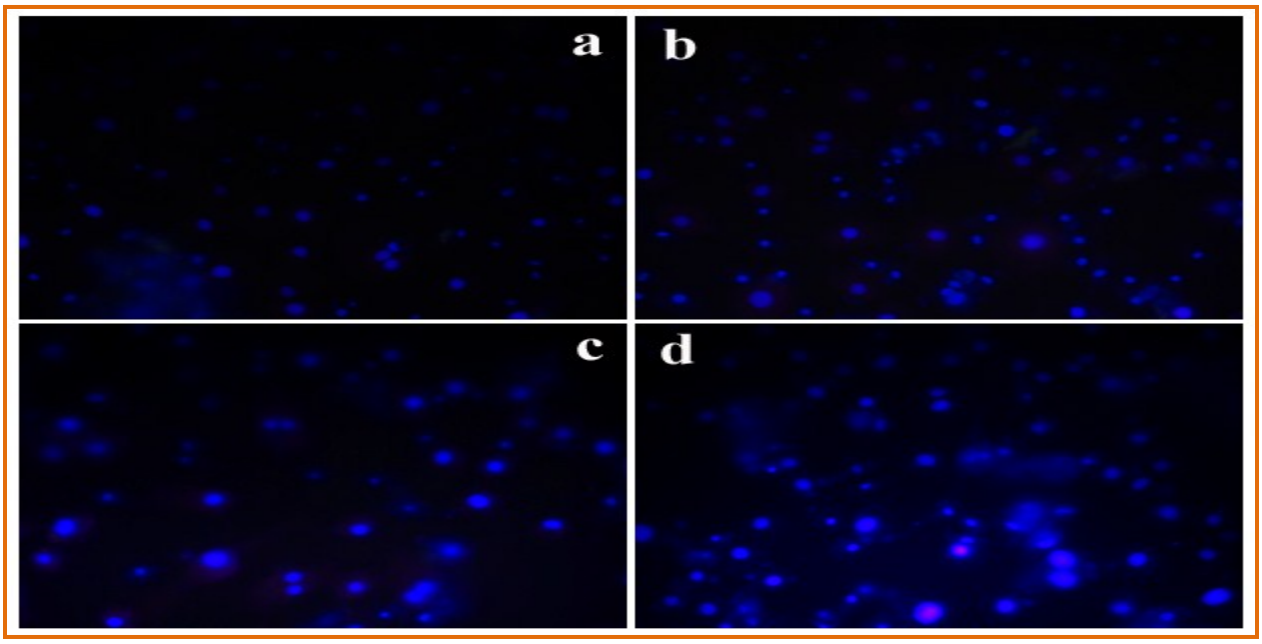

Fig. S36 Nuclear morphology of HepG2 cells stained with DAPI. HepG2 cells were treated with the positive control *cisplatin* for 24 h and stained with DAPI. (a) Control; (b), (c), (d) After 24 h treatment with 5 µM, 10 µM and 20 µM respectively.

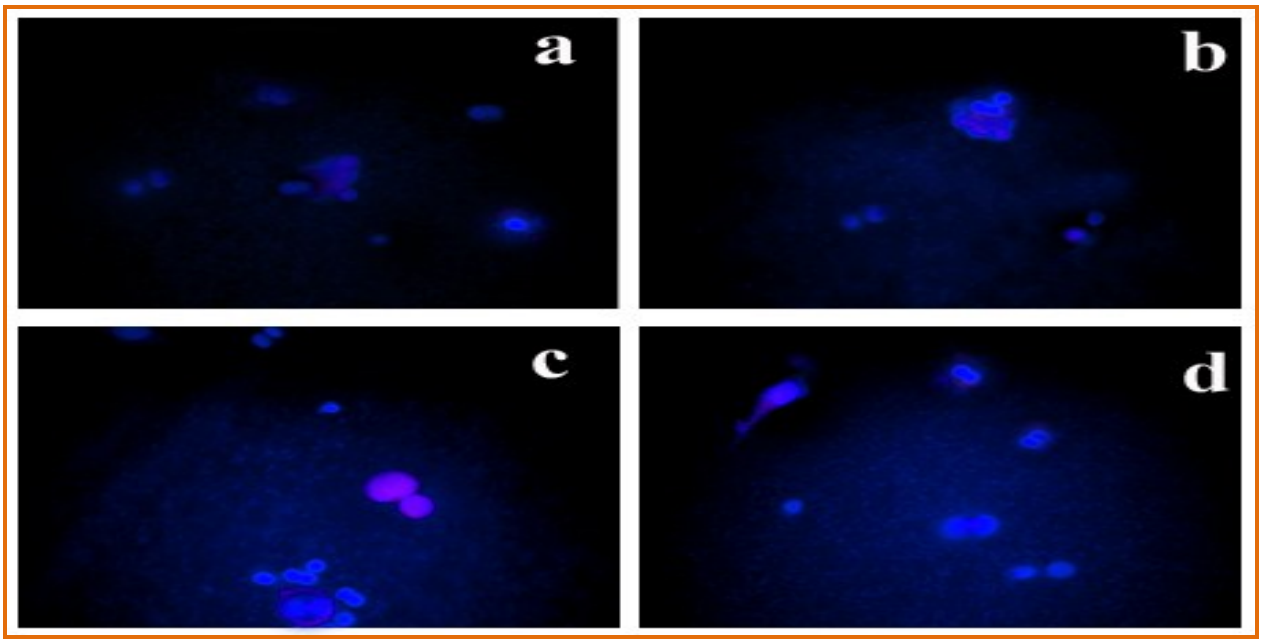

Fig. S37 Nuclear morphology of HT-29 cells stained with DAPI. HT-29 cells were treated with the positive control *cisplatin* for 24 h and stained with DAPI. (a) Control; (b), (c), (d) After 24 h treatment with 5 μM, 10 μM and 20 μM respectively.

Table S1 Crystallographic data of the complex **3**

Identification code	**[{Pd(3MAC-etsc)}$_4$] (3)**
Empirical formula	$C_{56}H_{52}N_{12}O_8Pd_4\ S_4$
Formula weight	1574.93
Temperature	100(2) K
Wavelength	0.7107 Å
Crystal system	Triclinic
Space group	P-1
Unit cell dimensions	
a	15.050(16)Å
b	15.307(16)Å
c	17.034 (18) Å
α	96.49(3)°
β	95.70(3)°
γ	114.56(2)°
Volume	3499 (6) Å^3
Z	2
Density	1.495 Mg/m^3
Absorption coefficient,	1.185 mm^{-1}
F(000)	1568
θ range for data collection	2.889 to 25.020 °
Limiting indices	-17≤*h*≤17, -17≤*k*≤17, -19≤*l*≤19
Reflections collected	35302
Independent reflections	11507 (*R*(int) = 0.2951)
Absorption correction	multi-scan
Refinement method	Full-matrix least-squares on F^2
Data / restraints / parameters	11507/ 1333/764
Goodness-of-fit on F^2	1.018
Final *R* indices [$I>2\sigma(I)$]	R1 = 0.1236, wR2 = 0.2552
R indices (all data)	R1 = 0.2560, wR2 = 0.3128

Table S2 Selected bond lengths (Å) and bond angles (°) of the complexes (**1-4**)

BOND LENGTHS							
1		**2**		**3**		**4**	
Pd(1)-N(1)	2.006(5)	Pd(1)-N(1)	1.998(4)	Pd(1)-N(1)	2.035(16)	Pd(1)-N(1)	2.004(1)
Pd(1)-C(1)	2.071(6)	Pd(1)-C(1)	2.065(5)	Pd(1)-C(1)	2.095(17)	Pd(1)-O(2)	2.045(2)
Pd(1)-S(1)	2.349(16)	Pd(1)-S(1)	2.346(1)	Pd(1)-S(1)	2.397(5)	Pd(1)-S(1)	2.2105(7)
Pd(1)-S(4)	2.352(17)	Pd(1)-S(4)	2.344(1)	Pd(1)-S(4)	2.396(6)	Pd(1)-Cl(1)	2.2989(3)
Pd(1)-Pd(1)	3.203(11)	Pd(1)-Pd(1)	3.172(7)	Pd(1)-Pd(1)	3.247(4)	-	-
BOND ANGLES							
1		**2**		**3**		**4**	
N1-Pd1-C1	80.8(2)	N1-Pd1-C1	80.9(2)	N1-Pd1-C1	80.8(7)	N1-Pd1-Cl1	177.02(5)
N1-Pd1-S1	82.46(15)	N1-Pd1-S1	82.9(1)	N1-Pd1-S1	83.7(4)	Cl1-Pd1-S1	90.88(2)
C1-Pd1-S1	162.19(19)	C1-Pd1-S1	161.6(1)	C1-Pd1-S1	163.8(6)	Cl1-Pd1-O2	89.09(4)
N1-Pd1-S1#1	174.96(15)	N1-Pd1-S1#1	174.4(1)	N1-Pd1-Pd2	94.93(5)	S1-Pd1-O2	179.39(4)
C1-Pd1-S1#1	104.23(19)	C1-Pd1-S1#1	104.6(1)	C1-Pd1-S4	104.9(6)	S1-Pd1-N1	86.73(5)
S1-Pd1-S1#1	92.51(4)	S1-Pd1-S1#1	91.95(5)	N1-Pd1-S4	173.2(5)	O2-Pd1-N1	93.29(6)
N1-Pd1-Pd1#2	90.43(15)	N1-Pd1-Pd1#2	88.9(1)	N1-Pd1-Pd2	121.6(1)	Pd1-N1-N2	118.5(1)
C1-Pd1-Pd1#2	91.49(16)	C1-Pd1-Pd1#2	93.1(1)	C1-Pd1-Pd2	86.0(5)	N1-Pd1-Cl1	177.02(5)
S1-Pd1-Pd1#2	94.66(4)	S1-Pd1-Pd1#2	95.12(4)	S1-Pd1-Pd2	100.2(1)	Cl1-Pd1-S1	90.88(2)
S1#1-Pd1-Pd1#2	89.76(4)	S1#1-Pd1-Pd1#2	89.38(4)	S4-Pd2-Pd1	89.93(1)	Cl1-Pd1-O2	89.09(4)
C11-S1-Pd1	95.2(2)	C11-S1-Pd1	94.3(2)	S1-Pd1-S4	90.2(2)	S1-Pd1-O2	179.39(4)
C11-S1-Pd1#3	105.5(2)	C11-S1-Pd1#3	103.0(2)	C15-Pd2-Pd1	94.3(6)	S1-Pd1-N1	86.73(5)
Pd1-S1-Pd1#3	114.46(7)	Pd1-S1-Pd1#3	114.54(6)	N4-Pd2-S3	173.8(4)		
N1-Pd1-C1	80.8(2)	N1-Pd1-C1	80.9(2)	N4-Pd2-C15	79.3(8)		
N1-Pd1-S1	82.46(15)	N1-Pd1-S1	82.9(1)	N4-Pd2-S2	85.0(4)		
C1-Pd1-S1	162.19(19)	C1-Pd1-S1	161.6(1)	C15-Pd2-S2	163.6(1)		
N1-Pd1-S1#1	174.96(15)	N1-Pd1-S1#1	174.4(1)	C29-Pd3-N7	80.9(8)		
C1-Pd1-S1#1	104.23(19)	C1-Pd1-S1#1	104.6(1)	N7-Pd3-S1	173.9(5)		
S1-Pd1-S1#1	92.51(4)	S1-Pd1-S1#1	91.95(5)	S1-Pd3-S3	92.0(2)		
N1-Pd1-Pd1#2	90.43(15)	N1-Pd1-Pd1#2	88.9(1)	C43-Pd4-N10	82.0(8)		
C1-Pd1-Pd1#2	91.49(16)	C1-Pd1-Pd1#2	93.1(1)	N10-Pd4-S2	172.7(4)		
S1-Pd1-Pd1#2	94.66(4)	S1-Pd1-Pd1#2	95.12(4)	N10-Pd4-S4	81.4(4)		
S1#1-Pd1-d1#2	89.76(4)	S1#1-Pd1-Pd1#2	89.38(4)	S1-Pd1-Pd3	110.9(2)		
C11-S1-Pd1	95.2(2)	C11-S1-Pd1	94.3(2)	Pd2-S3-Pd3	112.7(2)		
C11-S1-Pd1#3	105.5(2)	C11-S1-Pd1#3	103.0(2)	Pd2-S2-Pd4	93.8(2)		
Pd1-S1-Pd1#3	114.46(7)	Pd1-S1-Pd1#3	114.54(6)	Pd1-S1-Pd4	112.2(2)		

Table S3 Hydrogen bonds for complexes **1-4** [Å and °]

D–H···A	d(D–H)	d(H···A)	d(D···A)	<(DHA)
[{Pd(3MAC-tsc)}$_4$] (**1**)				
C2B-H2B1...O1A#4	0.98	2.39	3.28(2)	151.1
C2B-H2B2...N2	0.98	2.58	3.531(17)	164.8
N3-H3NA...O1B	0.82(7)	2.12(9)	2.94(5)	177(7)
N3-H3NA...O1B#5	0.82(7)	2.33(8)	3.15(4)	172(6)
N3-H3NB...O2#6	0.84(9)	2.14(9)	2.971(8)	172(8)
Symmetry operation: (**y+1/4, -x+3/4, -z+3/4); (-x+1, -y+1/2, z+0); (-y+3/4, x-1/4, -z+3/4); (-x+1, -y+1, -z+1); (-x+0, -y+1/2, z+0); (y-1/4, -x+3/4, z-1/4)**				
[{Pd(3MAC-mtsc)}$_4$] (**2**)				
N(3)-H...O(2)	0.880	2.09(7)	2.891(6)	149.4
Symmetry operation**: (x, y, z); (1/2-x, -y, 1/2+y); (3/4-y, 1/4+x, 1/4+z); (3/4+y, 3/4-x, 3/4+z); (1/2+x, 1/2+y, ½+z); (-x, 1/2-y, z); (1/4-y; 3/4+x; ¾+z); (1/4+y;1/4-x;1/4+z); (-x,-y, -z); (1/2+x, y, ½-z); (1/4+y, 3/4-x, 3/4-z); (1/4-y, 1/4+x,1/4-z); (1/2-x, 1/2-y, ½-z); (x, 1/2+y; -z); (3/4+y, 1/4-x, 1/4-z); (3/4-y, 3/4+x; 3/4-z)**				
[{Pd(3MAC-etsc)}$_4$] (**3**)				
N(12)-H(12)...O(2)	0.880	2.059	2.922	9.64
N(6)-H(6)...O(8)	0.880	2.184	2.848	34.71
Symmetry operation**: (x, y, z); (-x,-y, -z);**				
[Pd(H-3MAC-ptsc)Cl] (**4**)				
N(3)-H(3)...O(3)	0.820	2.040	2.858	174.56
Symmetry operation**: (x, y, z); (1/2-x, 1/2+y, 1/2-z); (1/2+x, 1/2-y, 1/2+z); (-x,-y, -z)**				

Table S4 Three-dimensional fluorescence spectral characteristics of BSA/HSA and BSA/HSA-Complexes systems

Compounds	**Rayleigh scattering peaks**			**Fluorescence peaks**		
	Peak position $\lambda_{ex}/\lambda_{em}$ (nm/nm)	**Stokes Δλ(nm)**	**Intensity (F)**	**Peak position $\lambda_{ex}/\lambda_{em}$ (nm/nm)**	**Stokes Δλ(nm)**	**Intensity (F)**
BSA						
BSA	280/280	0	637.73	280/343	63	514.37
BSA+ **[H_2-3MAC-tsc]**	280/280	0	710.98	280/341	61	498.91
BSA+ **[H_2-3MAC-mtsc]**	280/280	0	669.64	280/341	61	457.95
BSA+ **[H_2-3MAC-etsc]**	280/280	0	661.26	280/342	62	429.53
BSA+ **[H_2-3MAC-ptsc]**	280/280	0	747.76	280/344	64	471.34
BSA+**1**	280/280	0	775.35	280/339	59	390.79
BSA+**2**	280/280	0	736.92	280/339	59	355.05
BSA+**3**	280/280	0	714.87	280/337	57	276.44
BSA+**4**	280/280	0	707.34	280/348	68	494.69
HSA						
HSA	280/280	0	480.02	280/333	53	289.67
HSA+ **[H_2-3MAC-tsc]**	280/280	0	493.18	280/333	53	242.36
HSA+ **[H_2-3MAC-mtsc]**	280/280	0	491.98	280/337	57	279.19
HSA+ **[H_2-3MAC-etsc]**	280/280	0	549.64	280/333	53	254.76
HSA+ **[H_2-3MAC-ptsc]**	280/280	0	550.23	280/333	53	264.30
HSA+**1**	280/280	0	633.52	280/334	54	261.04
HSA+**2**	280/280	0	613.07	280/332	52	263.30
HSA+**3**	280/280	0	782.63	280/327	47	255.36
HSA+**4**	280/280	0	697.72	280/330	50	269.07